Acta Geologica Sinica (English Edition), 2023, 97(2): 526–547

Sedimentary Processes and Depositional Characteristics of Coarse-grained Subaqueous Fans along Steep Slopes in a Lacustrine Rift Basin: A Case Study from the Dongying Depression, Bohai Bay Basin, China

YANG Baoliang[1], QIU Longwei[1, 2, *], YANG Yongqiang[1, 2], Kouassi Louis KRA[1], DONG Daotao[1] and Danish KHAN[1, 3]

[1] *School of Geosciences, China University of Petroleum (East China), Qingdao, Shandong 266580, China*
[2] *Key Laboratory of Deep Oil and Gas in China University of Petroleum (East China), Qingdao, Shandong 266580, China*
[3] *State Key Laboratory of Ore Deposit Geochemistry, Institute of Geochemistry, Chinese Academy of Sciences, Guiyang, Guizhou 550081, China*

Abstract: Coarse-grained subaqueous fans are vital oil and gas exploration targets in the Bohai Bay basin, China. The insufficient understanding of their sedimentary processes, depositional patterns, and controlling factors restricts efficient exploration and development. Coarse-grained subaqueous fans in the Yong′an area, Dongying Depression, are investigated in this study. These fans include nearshore subaqueous fans, and sublacustrine fans, and their sedimentary processes, depositional patterns and distribution characteristics are mainly controlled by tectonic activity and paleogeomorphology. Nearshore subaqueous fans developed near the boundary fault during the early–middle deposition stage due to strong tectonic activity and large topographic subsidence. Early sublacustrine fans developed at the front of the nearshore subaqueous fans in the area where the topography changed from gentle to steep along the source direction. While the topography was gentle, sublacustrine fans did not develop. During the late weak tectonic activity stage, late sublacustrine fans developed with multiple stages superimposed. Frequent fault activity and related earthquakes steepened the basin margin, and the boundary fault slopes were 25.9°–34°. During the early–middle deposition stage, hyperpycnal flows triggered by outburst floods developed. During the late deposition stage, with weak tectonic activity, seasonal floods triggered hyperpycnal flows, and hybrid event beds developed distally.

Key words: sedimentary processes, depositional characteristics, paleogeomorphology, coarse-grained subaqueous fan, lacustrine rift basin, Dongying Depression

Citation: Yang et al., 2023. Sedimentary Processes and Depositional Characteristics of Coarse-grained Subaqueous Fans along Steep Slopes in a Lacustrine Rift Basin: A Case Study from the Dongying Depression, Bohai Bay Basin, China. Acta Geologica Sinica (English Edition), 97(2): 526–547. DOI: 10.1111/1755-6724.14994

1 Introduction

Mesozoic and Cenozoic continental rift lacustrine basins are essential types of petroliferous basins in eastern China (Cao et al., 2018). Due to their proximity to the provenance area and the fault activity that caused the steep topography, coarse-grained sedimentary bodies formed easily (Zhu et al., 2018). Coarse-grained subaqueous fans are adjacent to deep lacustrine source rocks, which have an excellent matching source-reservoir-caprock relationships, and they are conducive to forming lithologic or structural-lithologic reservoirs with excellent exploration potential (Wang et al., 2016). As the onshore hydrocarbon-bearing basins in eastern China transitioned from the stage of subtle hydrocarbon exploration to the stage of high exploration degree, the coarse-grained subaqueous fan reservoirs developed along the steep slopes of the lacustrine rift basin, and are among the main targets for hydrocarbon exploration and development in the Jiyang Subbasin (Xian et al., 2007; Song, 2018; Wang, 2021; Zhong et al., 2022). However, coarse-grained sediments have characteristically large vertical thicknesses, multiphase superposition, rapid lateral lithologic changes, and complex oil-water relationships (Sui et al., 2010; Liu Q H et al., 2020). Insufficient understanding of the internal architecture characteristics and distribution patterns severely restricts reservoirs' exploration and exploitation processes.

A series of factors controlling the internal architecture characteristics and distribution patterns of coarse-grained sediment have been proposed in previous research work, such as tectonic activity, base-level fluctuations, and climate variations, which affect generation, transport, and deposition (Xian et al., 2007; Cao et al., 2018; Liu L et al., 2020; Li et al., 2021; Ma et al., 2021; Yu et al., 2021). Tectonic activity factors play a key role in sedimentary filling in lacustrine rift basins (Deng et al., 2001; Lin,

* Corresponding author. E-mail: qiulwsd@163.com

http://www.geojournals.cn/dzxbcn/ch/index.aspx; https://onlinelibrary.wiley.com/journal/17556724

2004; Henstra et al., 2016; Liu et al., 2019; Zhang et al., 2019). A large number of previous studies on fault-controlled sedimentary systems have enhanced our understanding of the internal structure and development pattern of coarse-grained sediments in rift basins (Cao et al., 2018; Chiarella et al., 2021; Yang B L et al., 2021; Dong et al., 2022). Cao et al. (2018) anatomized the internal architectures and sedimentary processes of nearshore subaqueous fans based on core observations and flume simulation experiments on the northern steep slope zone of the Minfeng Sag in the northeast part of the Dongying Depression, and they proposed a fault-controlled non-channelized nearshore subaqueous fan deposition model. Chiarella et al. (2021) analyzed the evolution model and factors controlling base-of-scarp deposits, representing the early unsteady conditions of fault-controlled systems. Different positions along the boundary and the difference in the intensity of fault activity affect the genetic type and depositional characteristics of coarse-grained sediments (Yang B L et al., 2021). Some scholars have also recognized that the sedimentary processes, genetic types and sedimentary patterns of subaqueous fans are controlled by tectonic activity, climate change, and also affected by differences in sedimentary topography, and sediment supply (Dong and He, 2016; Zhang et al., 2019; Yu et al., 2021). In a complicated continental rift basin, paleogeomorphology controlling sand body mechanisms contain ditch-valley and slope break belts that affect sand bodies development (Deng et al., 2001; Wang et al., 2003; Zhang et al., 2003; Lin, 2004; Feng, 2006; Dong et al., 2018). The supply mode and nature of parent rocks in the source area of paleomorphic elements directly affect the size and rock type of sedimentary sand bodies (Dong and He, 2016). Therefore, it is essential to clarify the main factors controlling the development of coarse-grained sediments and how these factors affect spatial and temporal distribution predictions.

The Dongying Depression is a Cenozoic intracontinental rift basin that is part of a secondary negative structural unit in the Jiyang Subbasin of the Bohai Bay Basin (Feng et al., 2013; Li et al., 2021). The early Paleogene strata were continuously buried, with sediment thicknesses exceeding 2000 m, and they entirely recorded the evolution of the boundary fault-controlled systems (Feng et al., 2013; Li et al., 2021). The main boundary-controlling fault in the Dongying Depression is the Chennan fault, and along its different positions, it has different tectonic subsidence rates in the same stage (Zhang et al., 2017). At different stages of tectonic evolution or different locations along the boundary fault zone, sedimentary processes, internal architectures and controlling factors of fault-controlled coarse-grained subaqueous fans are still in the initial research stage. With the increase in exploration and development activities, the study of related contents has gradually become a bottleneck for effectively evaluating and predicting high-quality reservoirs in the study area. This paper takes the coarse-grained subaqueous fans developed on the northern steep slopes of the Yong′an area, Dongying Depression, as the research objects, and aims to (1) better understand the internal architecture of the coarse-grained subaqueous fans, (2) reveal the sedimentary processes under different tectonic activities and geomorphological conditions during different deposition stages, and (3) analyze the factors that control the development of coarse-grained subaqueous fans in the steep slope belt, and establish a depositional model. This work is of important theoretical and application significance for the further exploration of coarse clastic reservoirs in the study area, and it serves as a reference for the exploration of analogous reservoirs in continental rift lacustrine basins.

2 Geological Setting

Located in the southeastern portion of the Jiyang Subbasin, Bohai Bay Basin, the Dongying Depression is a northeast–southwest-trending half-graben that extends 65 km from east to west and 90 km from north to south and covers an area of 5700 km^2 (Fig. 1a, b) (Feng et al., 2013; Liu J P et al., 2017; Cao et al., 2018). The depression is bordered to the east by the Qingtuozi uplift, to the west by the Pingnan fault and the Gaoqing fault, to the north by the Chenjiazhuang uplift, to the south by the Qihe–Guangrao fault, and to the south by the Luxi and Guangrao uplifts (Fig. 1c) (Feng, 1999). The Dongying Depression is oriented from north to south, and the depression has a steep slope zone in the north, a depression in the north (Minfeng Depression), a central uplift zone, a depression in the south (Niuzhuang Depression) and a gently sloping zone in the south (Fig. 1d). The Yong′an area is the study area of this paper and is located in the eastern section of the northern steep slope zone of the Dongying Depression (Fig. 1c).

Two-stage tectonic evolution (65.0 Ma to Quaternary) mainly occurred in the Dongying Depression, which underwent Paleogene synrifting differential subsidence before 24.6 Ma, followed by Neogene post-rift thermal subsidence (Fig. 2) (Hu et al., 2001; Zhu et al., 2020). The Paleogene syn-rifting stage is composed of the early-initial rifting stage (65–50.4 Ma), the late-initial rifting stage (50.4–42.5 Ma), the rift climax stage (42.5–38 Ma), and the weakening rifting stage (38–24.6 Ma) (Feng et al., 2013). Paleogene strata in the Dongying Depression include the Kongdian Formation (E*k*), which is overlain by the Shahejie (E*s*) and Dongying (E*d*) formations. The strata of the Shahejie Formation (E*s*) comprise four parts, including Es_4, Es_3, Es_2 and Es_1 (Shang et al., 2022). The strata of Es_4 include the upper and lower parts (Fig. 2) (Li et al., 2021). During the upper member of Es_4 (Es_4^U) period, large amounts of terrigenous coarse-grained sediments from the Chenjiazhuang uplift were carried by mountain-derived floods into the lake and formed three types of sedimentary facies: nearshore subaqueous fan, fan delta and sublacustrine fan facies (Cao et al., 2018; Zhang et al., 2019).

3 Data and Methods

Sequence stratigraphic characteristics were analyzed using 3D seismic data merged with wireline log data and seismic synthetic records. Four types of seismic facies

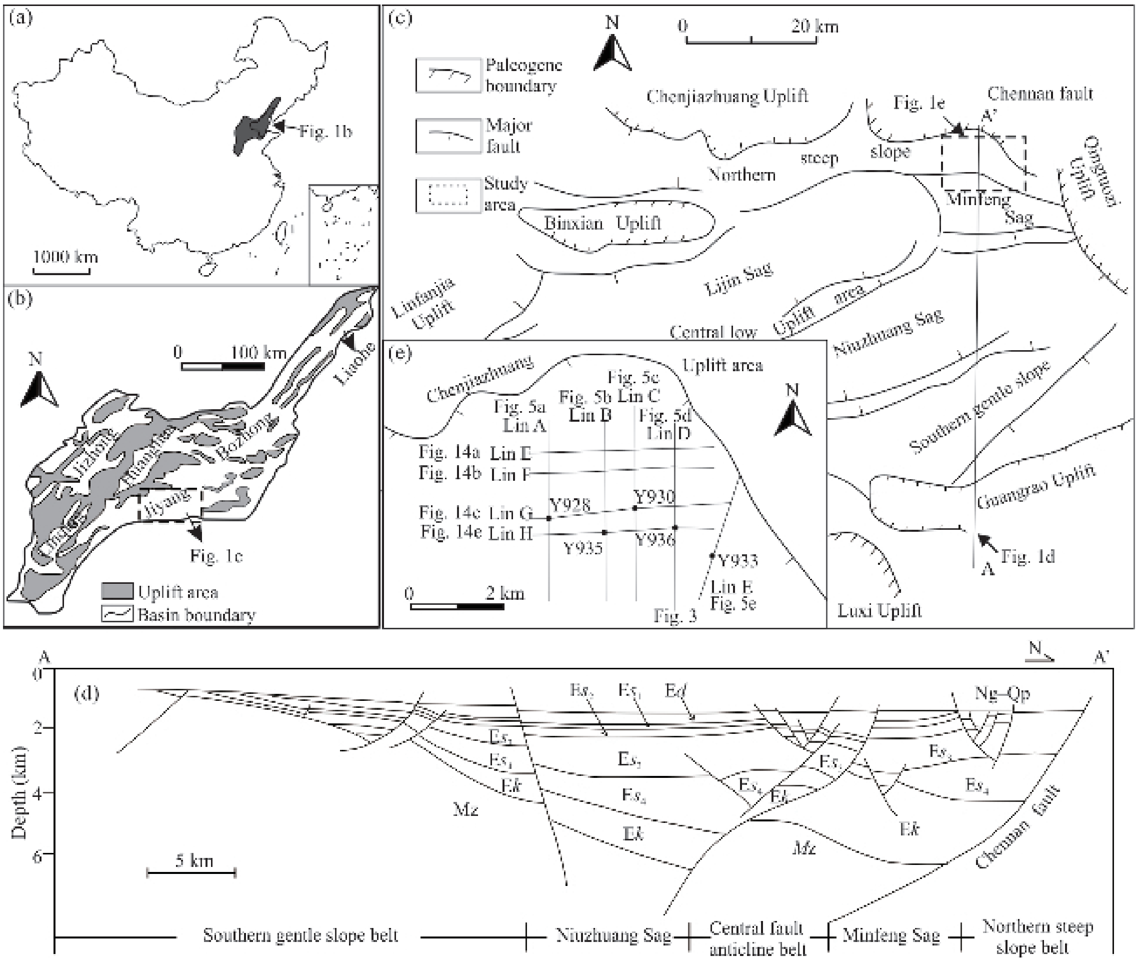

Fig. 1. Schematic map of the Dongying Depression, Bohai Bay Basin, eastern China (modified from Feng et al., 2013; Ma et al., 2016).

(a) Regional tectonic location of the Bohai Bay Basin in eastern China, China basemap after China National Bureau of Surveying and Mapping Geographical Information; (b) tectonic location of the Dongying Depression in the Jiyang Subbasin; (c) division of tectonic units in the Dongying Depression and the location of the Yong'an area; (d) interpretation of geological the profile corresponding to the measured line AA' in Fig. 1c; (e) well location map and measured line distribution in the study area.

were identified according to the reflection geometry and amplitude characteristics and stacking pattern of seismic reflections (Li et al., 2019). Stratigraphic horizons were interpreted using Geoframe software, and the closed-tracking seismic horizon data were used to make cumulative vertical displacement profiles along the Chennan fault, and they were imported into Petrel software to generate time isopach maps. Based on the seismic profile interpretation of the overwell, the dip angle of the boundary fault was calculated and combined with seismic synthetic records and trigonometric relationships. Core data from five wells containing the target section in the study area, with a cumulative core length of nearly 200 m, were observed. The depths of the target interval are between 3000 and 4000 m from the surface. The lithology, grain size, support mechanism and sedimentary structure characteristics were integrated to classify the lithofacies type. Based on the lithofacies interpretation and vertical facies sequence, sedimentary microfacies, fluid type and sedimentary process analyses were carried out. The root mean squared amplitude was extracted using seismic attributes. The planar distribution of the coarse-grained subaqueous fans was determined jointly by combining lithofacies distribution and seismic reflection characteristics. The relationship between the controlling factors, i.e., tectonic activity, climate, paleotopography, and parent rock type, as well as the depositional process, sedimentary structure and distribution pattern of the coarse -grained subaqueous fans in the steep slope zone of the rift lacustrine basin were discussed.

4 Results

4.1 Division of strata and depositional stages

According to the stratum stacking pattern, the strata of Es_4^{U} can be divided into three cycles, including Es_4^{U-1}, Es_4^{U-2}, and Es_4^{U-3} (Fig. 3). There are similarities in the seismic reflection structures within each cycle unit. The strata in the Es_4^{U-1} and underlying Es_4^{U-3} cycles are retrograded superimposed. The strata in the cycle Es_4^{U-2} are retrograded superimposed at its base, followed by prograded superimposed. This paper focuses on the Es_4^{U-3}

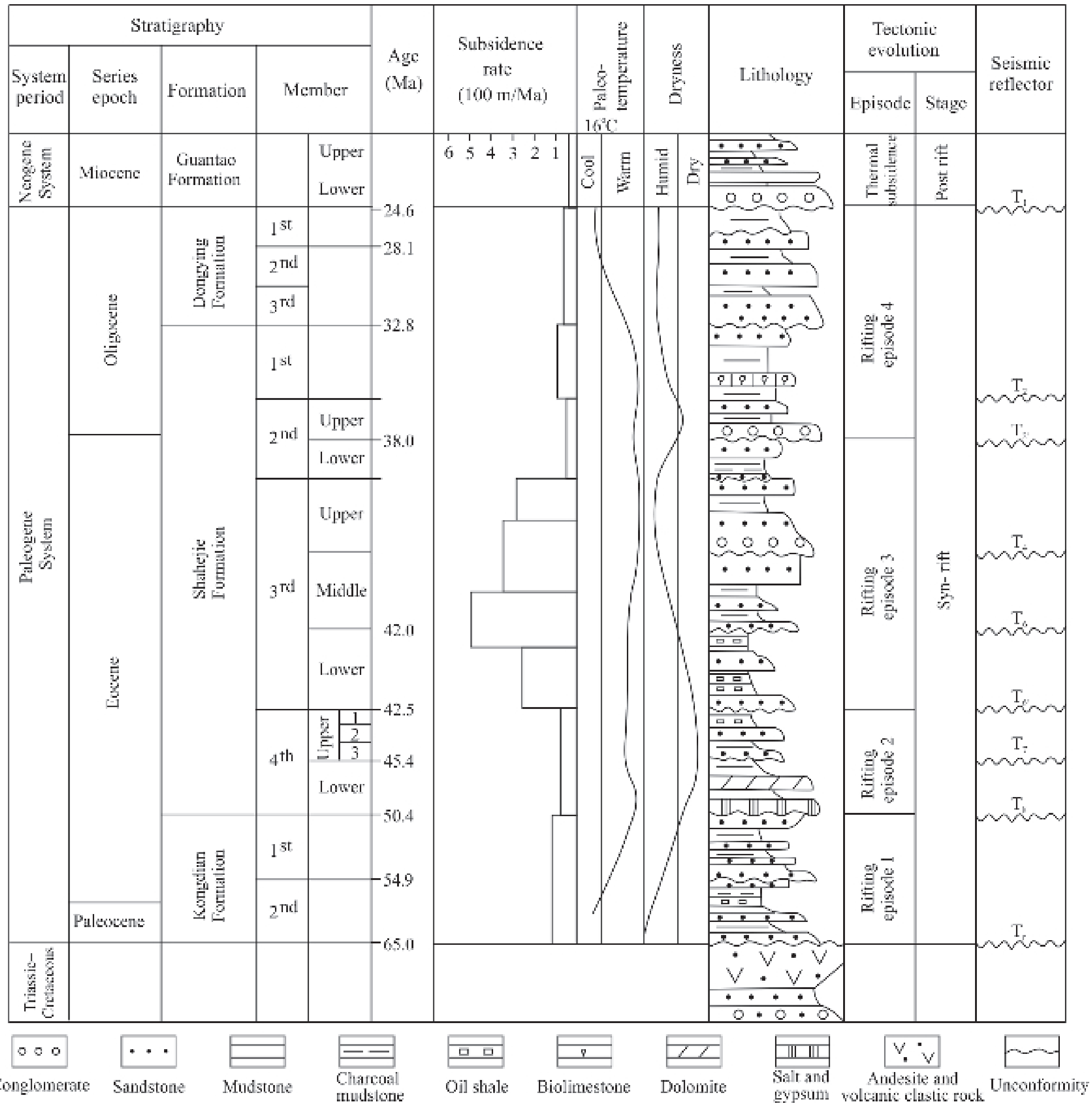

Fig. 2. General sequence stratigraphic charts and tectonic events of the Dongying Depression (modified from Feng et al., 2013; Li et al., 2021).

stage at the beginning of the Es_4^U, which corresponds to the late initial rifting stage.

According to the seismic reflection structure characteristics of coarse-grained subaqueous fans, the target interval is divided into three depositional stages: early, middle and late. Here we take the seismic section along the source direction in Fig. 3 as an example to introduce the difference in seismic reflection structures of coarse-grained subaqueous fans in different depositional periods. During the early deposition stage, coarse clastic deposits accumulated rapidly near the root of the boundary fault to form a wedge-shaped deposits. During the middle deposition stage, retrograde reflection developed over the wedge-shaped deposits. Multi-stage distant lenticular reflections developed in the deep lake during the late deposition stage.

4.2 Faults activity features

The depositional period of the studied interval corresponds to the late initial rifting stage of the Dongying Depression, and the subsidence process of the rift basin is characterized by episodic tectonic movements, with maximum tectonic subsidence rates of approximately 140–100 m/Ma (Lin, 2004; Feng et al., 2013). There are differences in the cumulative vertical displacement along the fault during the same period (Fig. 4), indicating that the fault activity rates along different locations of the Chenan fault are not synchronized. The maximum displacement in the middle section (wells Y935 and Y930 areas) is less than 192 ms, which is smaller than that in both the eastern (well Y928 area, up to 278 ms) and western sections (well Y936 area, up to 315 ms) (Fig. 4b). During the early–middle deposition stage, retrograded subaqueous fans developed in the western (well Y928

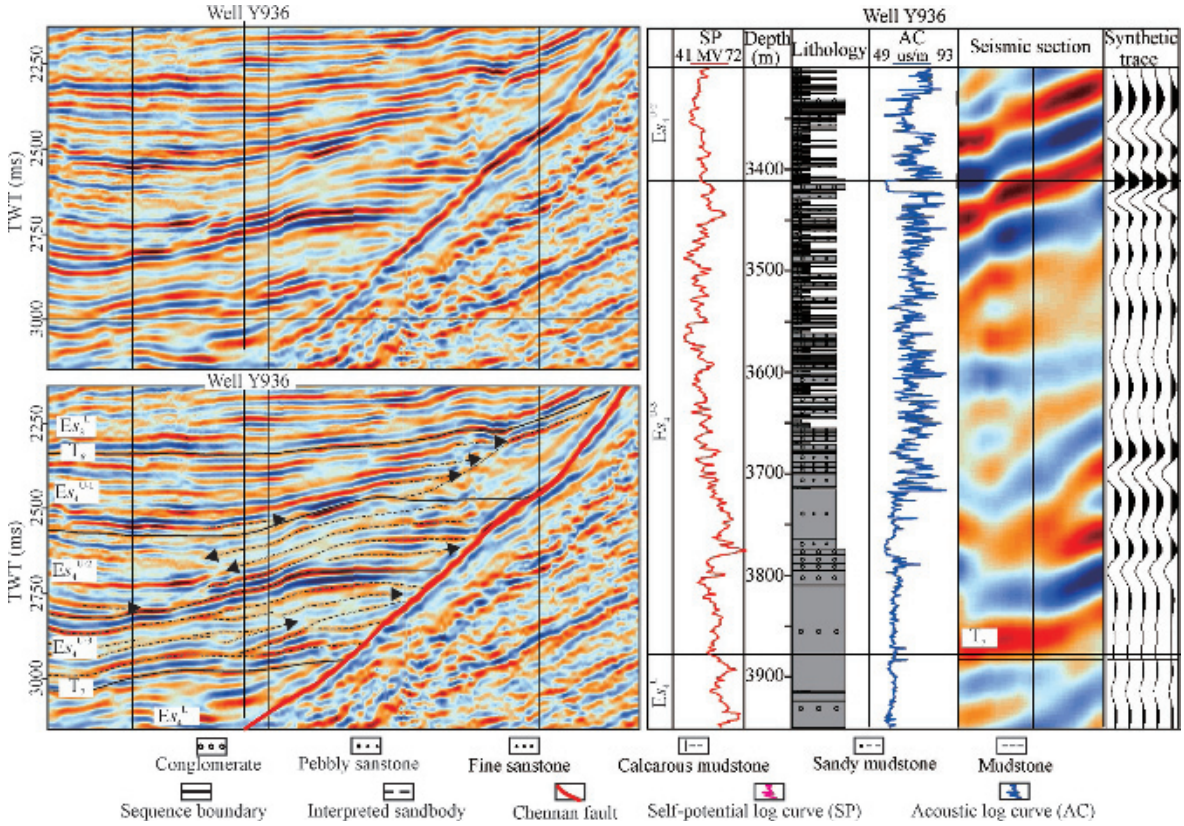

Fig. 3. Sequence stratigraphic framework and synthetic seismogram of well Y936 during the Es_4^{U-3} interval in the Yong'an area.

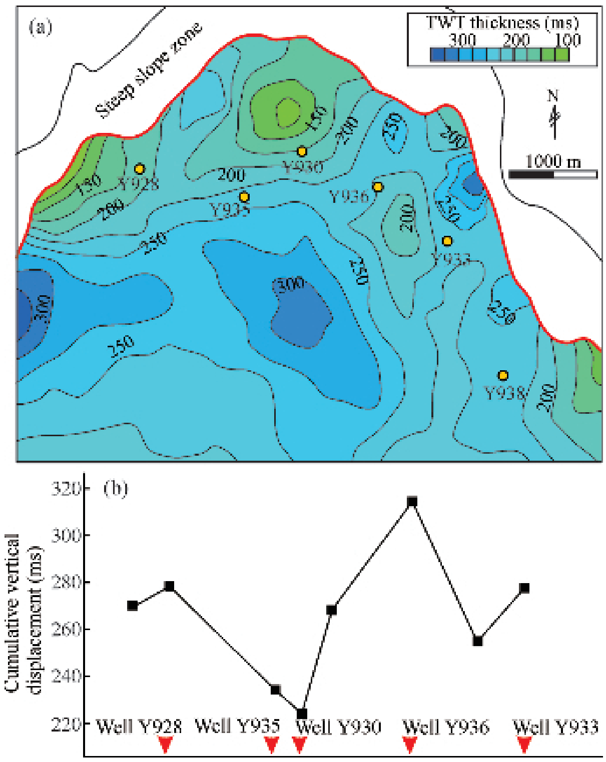

Fig. 4. (a) Time-thickness map of the Es_4^{U-3} period and the key representative wells; (b) the cumulative vertical displacement profiles along the Chennan fault during the Es_4^{U-3} stage.

area) and eastern (well Y936 area) sections (Fig. 5a, d), and progradeded subaqueous fans developed in the middle section (wells Y930 and Y935 areas; Fig. 5b, c), indicating that the tectonic subsidence rate is higher in the western and eastern sections than that in the middle section. The progradeded subaqueous fans developed in the low value of the cumulative vertical displacement may indicate the existence of relay ramps (Li et al., 2021; Ma et al., 2021).

The coarse clastic rocks deposited with large thickness and near-source accumulation during the early–middle sedimentary period, while those deposited during the late stage had small thickness and a long extension distance (Figs. 3, 5). The tectonic activity is strongly correlated with the sediment supply, accommodating space and the geomorphology of the catchment area (Liu et al., 2019; Li et al., 2021). The tectonic activity in the continental rift lacustrine basin is characterized by episodic tectonic movement, with rapid mechanical subsidence followed by more extended periods of tectonic quiescence (Martins-Neto and Catuneanu, 2010). Therefore, during the early–middle deposition stage, the strong sediment supply corresponds to the period of strong tectonic activity, and the weak sediment supply in the late stage corresponds to the weak tectonic activity period.

4.3 Type and characteristics of lithofacies

According to the characteristics of rock type, texture and sedimentary structures, 15 types of lithofacies were classified and summaried in Figs. 6, 7, and Table 1. Three broad lithofacies were delineated, including conglomerate

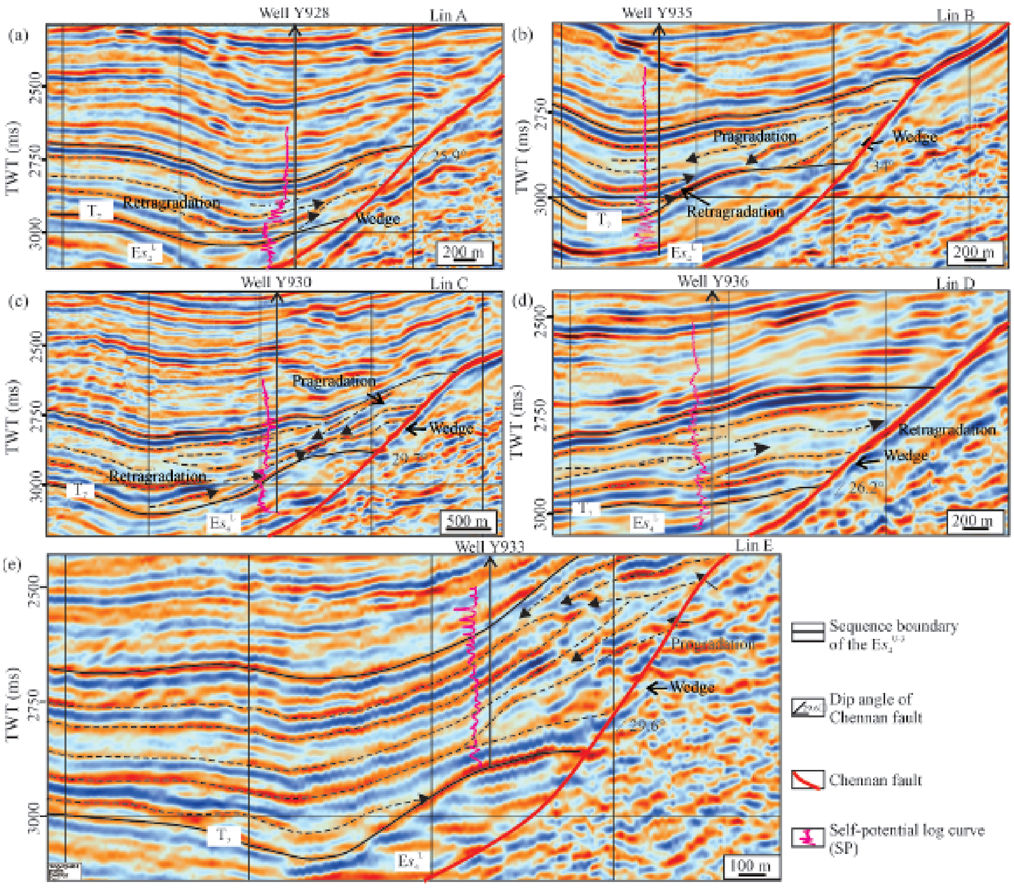

Fig. 5. Seismic profile along the source direction (profile location is shown in Fig. 1e).

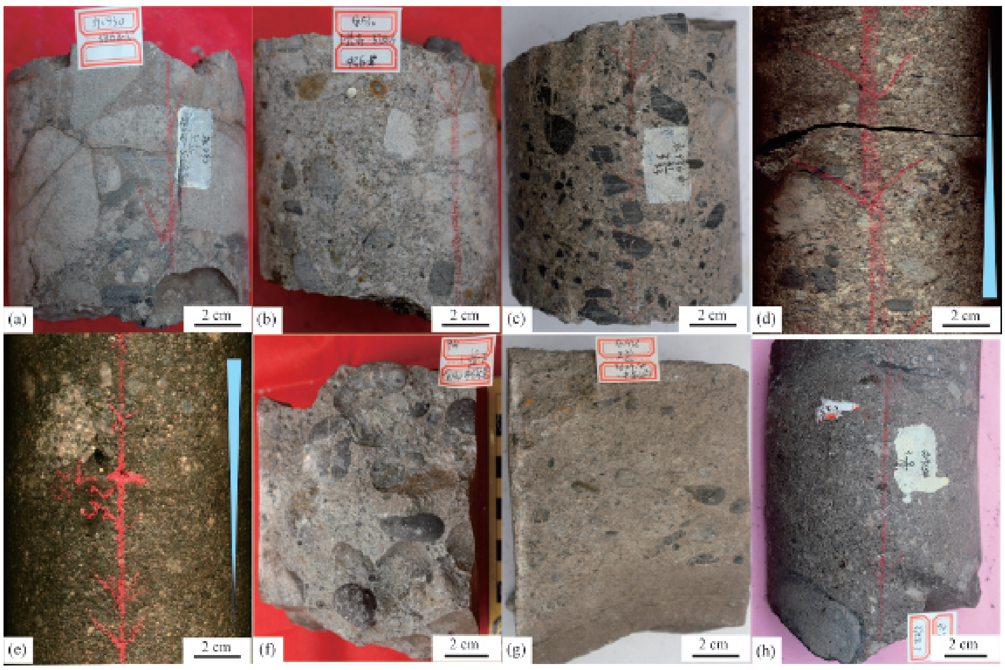

Fig. 6. Typical depositional characteristics of conglomerate facies.
(a) Grain-supported pebble conglomerate facies, 3862.5 m, well Y930; (b) matrix-supported pebble conglomerate facies, 3755.9 m, well Y930; (c) sandy matrix-supported pebbly fine conglomerate facies with angular gravels, 3794.9 m, well Y936; (d) normally graded bedding conglomerate facies, 3755.1 m, well Y930; (e) inversely graded conglomerate facies, 3845.15 m, well Y928; (f) imbricated pebble conglomerates facies, with subrounded to rounded gravels and imbricated arrangement, 3211.15 m, well Y933; (g) imbricated fine conglomerates facies, 3629.4 m, well Y936; (h) normally graded imbricated conglomerates facies, 3758.3 m, well Y928.

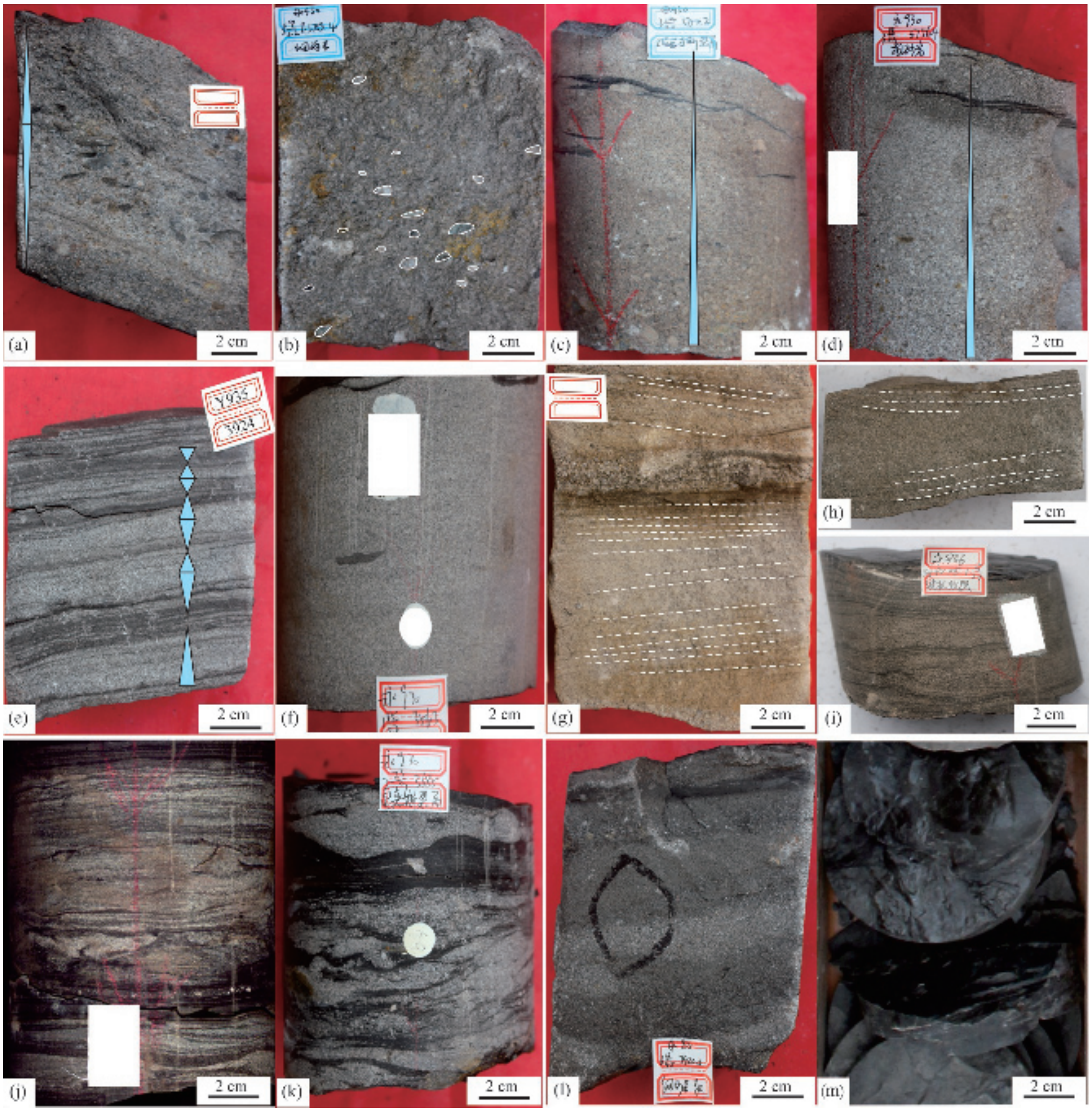

Fig. 7. Typical depositional characteristics of sandstone and mudstone facies.
(a) Graded pebbly sandstone facies, 3906.36 m, well Y935; (b) massive imbricated pebbly sandstone facies, 3753.4 m, well Y930; (c) normally graded pebbly sandstone-sandstone facies, 3754.4 m, well Y930; (d) normally graded sandstone facies, 3756.4 m, well Y930; (e) graded sandstone facies, 3924 m, well Y935; (f) massive fine-grained sandstone with rip-up mud clasts that are parallel along the bed, 3563 m, well Y930; (g) parallel-bedding sandstone facies accompanied cross-bedded sandstone facies, 3214.4 m, well Y933; (h) cross-bedded sandstone facies, 3627.9 m, well Y930; (i) rippled sandstone facies, 3492.05 m, well Y936; (j) rippled sandstone facies, 3563.8 m, well Y930; (k) clast-rich argillaceous sandstone facies, 3685 m, well Y930; (l) graded muddy sandstone with plant debris, 3920.5 m, well Y935; (m) black mudstone facies, 3632.25 m, well Y930.

facies, sandstone facies and mudstone facies. The conglomerate facies include massive conglomerate facies (MC), graded bedding conglomerate facies (GC), and imbricated conglomerate facies (Gi). The sandstone facies include imbricated pebbly sandstone facies (Spi), graded pebbly sandstone–sandstone facies (Gps), massive pebbly sandstone facies (Mps), graded sandstone facies (Gs), massive sandstone facies (Ms), parallel bedding sandstone facies (Ps), cross bedding sandstone facies (Cs), rippled bedding sandstone facies (Rs), clast-rich argillaeous sandstone facies (Cas), and muddy sandstone facies (Mss). The mudstone facies include sandy mudstones facies (Sm), and mudstones facies (M). The description of their lithological features and depositional environment is briefly discussed in Table 1.

4.4 Seismic reflection features and distribution of coarse-grain clastic rocks

4.4.1 Seismic reflection feature

There are four types of seismic facies in the studied interval, including wedge-shaped reflection facies, retrograded seismic facies, prograded seismic facies and lenticular reflection facies (Fig. 5). (1) For the wedge-shaped reflection facies, the outer geometry of the seismic

Table 1 Lithofacies types and characteristics

Facies code	Lithofacies	Features	Interpretation
MC	Massive conglomerate (Fig. 6a–c)	Massive structure, matrix- and clasts-supported, angular and sub-angular, poor sorted	Gravel-rich debris flows (Lowe, 1976; Sohn, 1997; Liu L et al., 2017)
GC	Graded bedding conglomerates (Fig. 6d, e)	Normal graded bedding and reverse graded bedding, matrix- and clasts-supported	Gravel-rich high-density turbidity currents (Lowe, 1982; Sohn, 1997)
Gi	Imbricated conglomerates (Fig. 6f–h)	Imbricated structures, scour and fill structures, structureless or graded bedding, matrix- and clasts-supported	Gravel-rich traction currents , bed-load (Zavala et al., 2011; Zavala, 2020)
Spi	Imbricated pebbly sandstone (Fig. 7a, b)	Imbricated structures, scour and fill structures, structureless or graded bedding, matrix- and clasts-supported	Sandy traction currents (Zavala et al., 2011; Zavala, 2020)
Gps	Graded pebbly sandstones-sandstones (Fig. 7c)	Normal graded bedding and inverse graded bedding	High-density turbidity currents (Lowe, 1982); Inverse graded bedding can be by formed by the kinetic sieving (Legros, 2002), dispersive pressure(Lowe, 1982), traction-carpet (Sohn, 1997), and vertical stacking of waxing flow (Zavala et al., 2011)
Gs	Graded sandstones (Fig. 7d, e)	Normal graded bedding and reverse graded bedding	Suspended-load, turbidity currents (Lowe, 1982)
Mps	Massive pebbly sandstones	Massive structure	Sandy debris flows (Shanmugam, 2012; Liu J P et al., 2017; Yang et al., 2019a)
Ms	Massive sandstones (Fig. 7f)	Massive structure	Sandy debris flows (Shanmugam, 2012; Liu J P et al., 2017; Yang et al., 2019a), or rapid fallout of unsorted, suspended material from the head of a turbulent flow(Henstra et al., 2016)
Ps	Parallel bedding sandstones (Fig. 7g)	Parallel bedding	Sandy traction currents (Zavala et al., 2011), Bouma Tb (Bouma, 1962; Liu L et al., 2017; Li et al., 2021)
Cs	Cross bedding sandstones (Fig. 7h)	Cross bedding	Sandy traction currents (Zavala et al., 2011)
Rs	Rippled bedding sandstones (Fig. 7i, j)	Rippled bedding	Sandy traction currents (Zavala et al., 2011), Bouma Tc (Bouma, 1962; Liu L et al., 2017; Li et al., 2021)
Cas	Clast-rich argillaceous sandstones (Fig. 7k)	Massive structure, graded bedding, sand matrix-supported, rip-up mud clasts,	Muddy debris flow (Liu J P et al., 2017), transitional flow (Haughton et al., 2009)
Mss	Muddy sandstones (Fig. 7l)	Massive structure, graded bedding	Suspended sediment
Sm	Sandy mudstones	Massive structure	Suspended sediment, mudflow (Bouma, 1962; Talling, 2012)
M	Mudstone (Fig. 7m)	Massive structure, horizontal bedding	Suspended sediment, low density turbidity current (Bouma, 1962; Talling et al., 2012)

reflection is wedge-shaped, and the inner geometry is blank or has weak reflections. The spontaneous potential (SP) log is box-shaped. (2) Retrograded seismic facies are deposited on the wedge-shaped reflection facies, and the SP log curve shows bell-shaped (Fig. 5a) or jagged box-shaped (Fig. 5d) geometries. (3) Prograded seismic facies consist of a set of prograded seismic reflectors with low to medium amplitudes and medium to high continuity. This facies is in angular contact with the underlying wedge-shaped seismic facies, corresponding to funnel-shaped signals in well logs (Fig. 5b, c, e). (4) The lenticular reflection facies show the characteristics of bidirectional downlap. This facies has medium-strong amplitudes and low-medium lateral continuity, with bell-shaped or finger-shaped signals in well logs.

4.4.2 Distribution of coarse-grain clastic rocks

During the early deposition stage, wedge-shaped reflection facies formed near the root of the boundary fault (Fig. 5). During the middle deposition stage, retrograded seismic facies developed overlying the wedge-shaped deposits in the east and in the western (well Y928 area) and eastern (well Y936 area) sections (Fig. 5a, d). In contrast, in both the middle section (wells Y930 and Y935 areas) and well Y933 area, prograded seismic facies developed in the proximal part and were accompanied by the development of retrograded seismic facies in the distal part (Fig. 5b, c, e). During the early–middle deposition stage, the fan shaped seismic attribute anomalies originate from the steep slope zone and can be interpreted as nearshore subaqueous fans (Fig. 8a). Fans developed at the distal end of the nearshore subaqueous fans, which can be interpreted as early sublacustrine fans (Fig. 8a). During the late deposition period, multi-stage lenticular reflection facies developed in the deep lake, which can be interpreted as late sublacustrine fans (Fig. 5a–d). On the plane, the late sublacustrine fans developed at the front of the nearshore subaqueous fans in the Y936, Y928 and Y930 well areas (Fig. 8).

5 Discussions

5.1 Two sedimentary facies types with different architectural units

5.1.1 Nearshore subaqueous fan

Nearshore subaqueous fans consist of wedge-shaped seismic facies, retrograded seismic facies, and prograded seismic facies in the dip direction.

In terms of seismic facies identification and core and logging data analysis, five types of sedimentary microfacies units are delineated: gravel-rich talus apron, main channel, braided channel, overbank, and lobe/sheet sands.

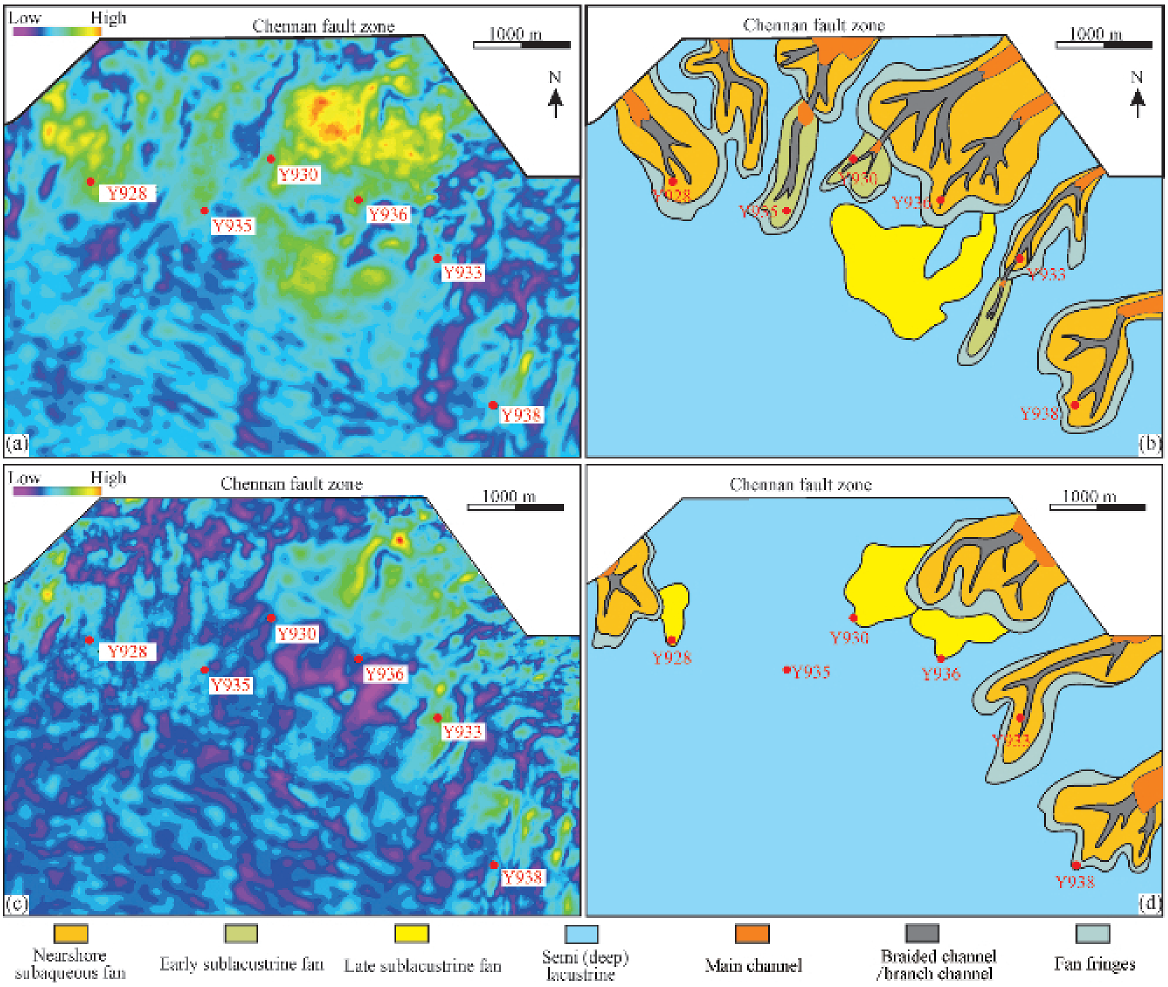

Fig. 8. RMS amplitude slices and corresponding interpretations of the sedimentary facies planar distribution during $Es_4^{U\text{-}3}$ interval.

5.1.1.1 Gravel-rich talus apron

Wedge-shaped seismic facies are developed adjacent to the bottom of the boundary faults (Fig. 5) and represent the talus at the base of the fault scarp (Surlyk, 1984). The clastic wedges are characterized by superimposed facies MC, with thicknesses up to 100 m; these strata have relatively low maturity and high matrix contents, are poorly sorted, have angular to subangular grain morphologies, and have no preferential orientation (Fig. 9a, b). The thick-bedded superimposed conglomerates are in abrupt contact with the lower and upper boundaries, which may have been formed by gravity-driven transport after a large-scale rock collapse along the fault scarp (Nemec, 1990; Henstra et al., 2016).

5.1.1.2 Main channel

The facies MC and Gi are dominant in the infills of the main channel, and the underlying fine-grained sediments are easily eroded. The gravels in facies MC are angular, poorly sorted and randomly distributed in the sandy matrix (Fig. 9c), indicating the "en masse" depositional process of plastic fluid (Lowe, 1976; Sohn, 1997; Liu L et al., 2017). Incidental coarse gravel is occasionally visible (Fig. 9d). The facies Gi consists of sandy supported fine to pebble conglomerates with subrounded to rounded, imbricately arranged gravels transported by bedload-dominated hyperpycnal flows (Zavala et al., 2011). The coarsening-upward sedimentary sequence in the prograded fans indicates an increase in flood energy intensity over time (Mulder et al., 2003; Zavala et al., 2011).

5.1.1.3 Braided channel

The vertical sedimentary sequence of the braided channel displays a vertical fining-up rhythm. Basal erosive contacts of the conglomerates with underlying sediments are common, indicating a confined channel depositional environment (Liu L et al., 2017). The proximal part of the braided channel is composed of facies MC (Fig. 10b), with overlying facies GC and Gps (Fig. 9f, g). The middle part consists of the facies Gi, Gs (Fig. 6g) and Spi (Fig. 10c), showing a vertical fining-upward trend. As the transport distance increases, the energy of the hyperpycnal flow weakens, its erosive ability on the underlying sediments weakens, and the complete sedimentary sequence can be preserved in the braided channel. The inverse to normal bedding sandstone facies is a typical sedimentary feature in hyperpycnal flows and can be found in the distal part

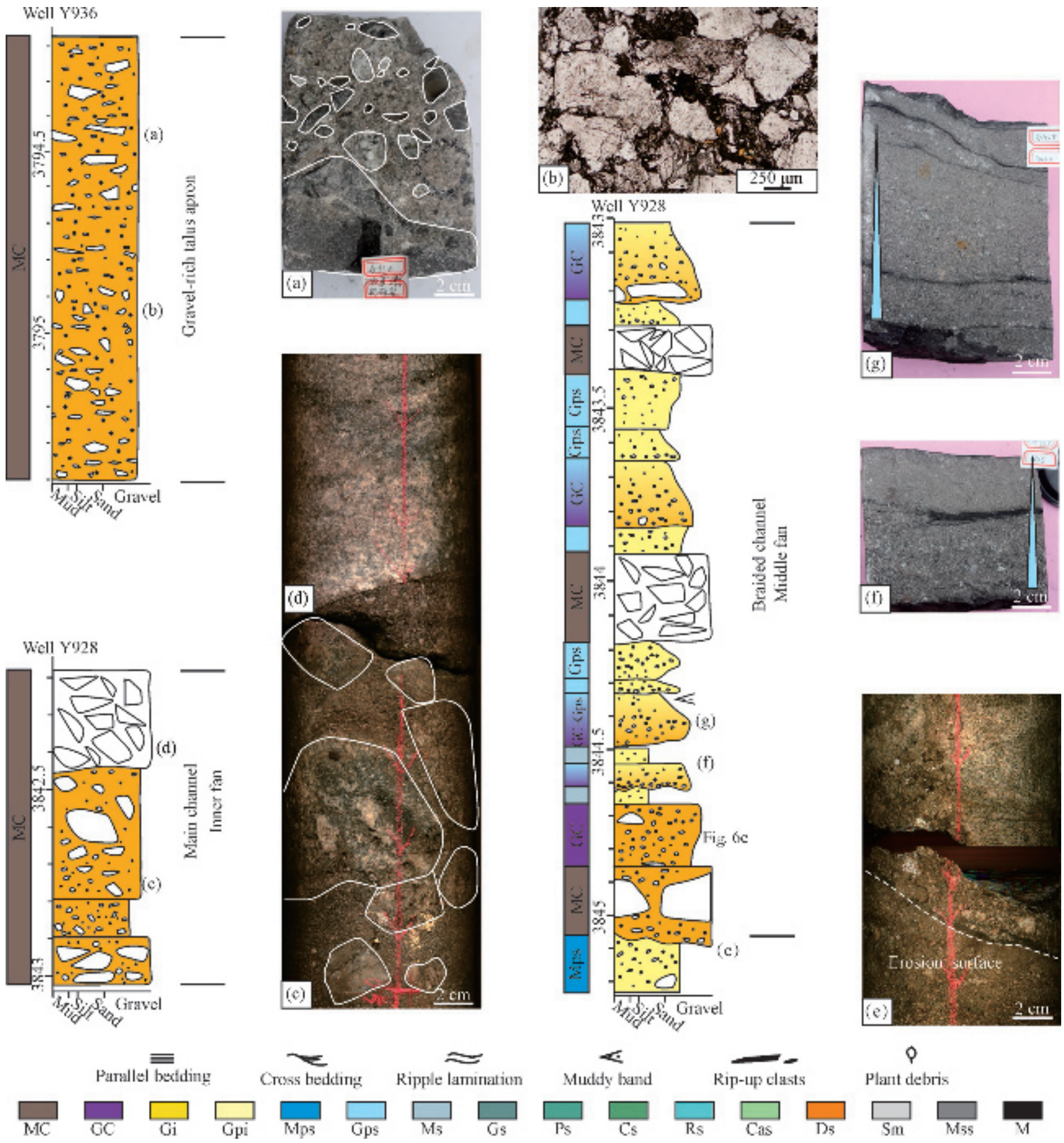

Fig. 9. Depositional characteristics of gravel-rich talus aprons, main channels, and braided channels of nearshore subaqueous fans.

(Fig. 10d) (Mulder et al., 2003; Zavala et al., 2011).

5.1.1.4 Overbank deposits

This sedimentary unit is distributed at the edge of the channel (Cao et al., 2018; Zhang et al., 2019). These sedimentary microfacies comprise facies Cs (Fig. 7h), Rs (Fig. 7e) and Gs. These facies are composed of gray fine- to coarse-graded sandstones with thicknesses of less than 0.15 m. They are interpreted as sand-rich traction deposits, which form by the gravitational sedimentation of suspended particles when the energy of the hyperpycnal flow is weak (Zavala et al., 2011).

5.1.1.5 Lobe/sheet sands

This sedimentary unit is filled predominantly by thick-bedded (approximately 0.7 m), well-sorted massive medium- to coarse-grained sandstones (Fig. 10f), presumably indicating the unloading of turbidity currents or debris flows at the end of the channel (Galloway, 1998; Posamentier and Kolla, 2003).

5.1.2 Sublacustrine fan

The early sublacustrine fan consists of retrograded seismic facies in the longitudinal section (Fig. 5b, c). The late sublacustrine fan shows lenticular seismic facies (Fig. 5a–c), medium–low amplitudes, and jagged-shaped signals in well logs. Based on a seismic reflection analysis, combined with core and logging data, four types of sedimentary microfacies can be identified: main channel, branch channel, overbank, and fan finger microfacies.

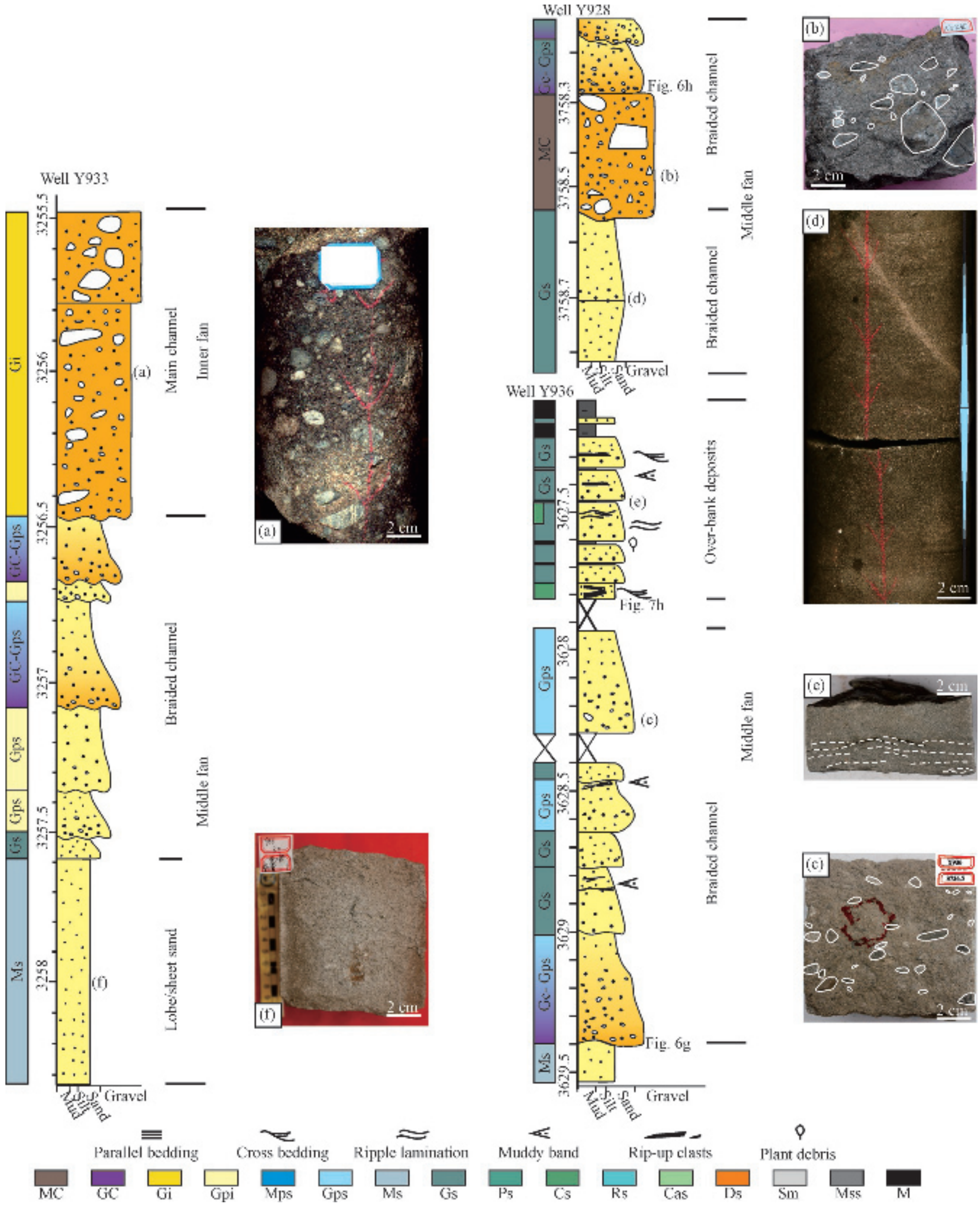

Fig. 10. Depositional characteristics of the braided channel and overbank deposits of the nearshore subaqueous fan.

5.1.2.1 Main channel

The near-source end of the main channel in the early sublacustrine fan consists of the facies Mc, with a stacked thickness exceeding 1 m. Its development far from the fault scarp suggests that it formed in a stage of strong flood energy against the background of tectonic activity (Fig. 11a) (Mulder et al., 2003; Liu et al., 2021). The relatively distal end of the main channel is composed of the facies Gi, with a stacked thickness exceeding 1 m. The higher roundness and sorting indicate a relatively farther transport distance.

The main channel of the late sublacustrine fans is composed of the facies Gi (Fig. 12a). The facies Gi is composed of fine conglomerate with a smaller superimposed thickness compared to that of early sublacustrine fans.

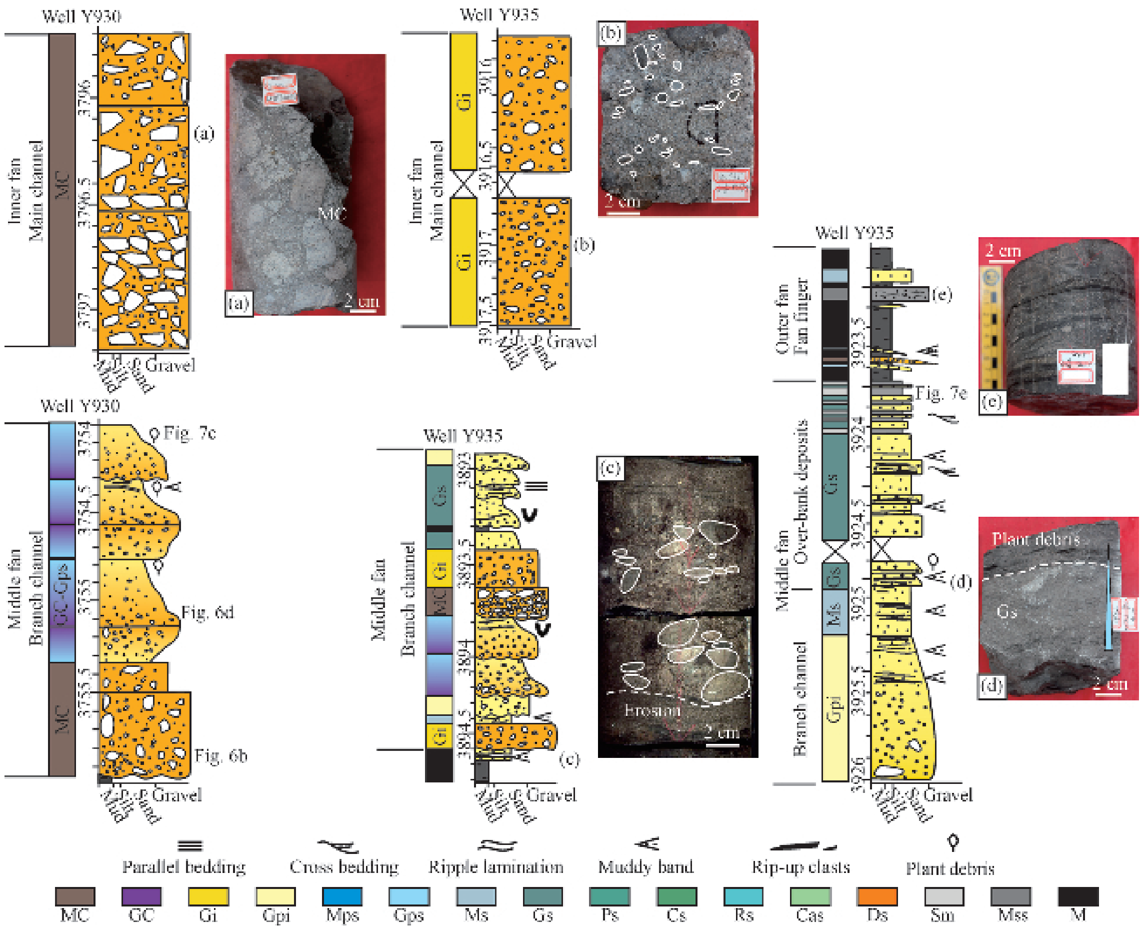

Fig. 11. Depositional characteristics of the early sublacustrine fan.

5.1.2.2 Branch channel

The braided channel is characterized by a vertical fining -up rhythm. The proximal part of the braided channel in the early sublacustrine fan comprises the facies MC (Figs. 6b, 10b), with the overlying facies GC and Gps. The overlying facies GC and Gps contain vertical fining-upward rhythms or compound inversely and normally graded rhythms, with black plant debris on the tops (Figs. 6d, 10c). The middle part is mainly composed of the facies Gi and GC-Gs (Fig. 11e), and the latter has a larger thickness. The front part is composed of the facies Spi and Gs.

The branch channel comprises facies Spi and Gs and contains vertical fining-upward rhythms or compound inversely normally graded rhythms, with black plant debris (Fig. 12b, c, d).

5.1.2.3 Overbank deposits

This sedimentary unit in the early sublacustrine fan comprises the facies Gs and Cs. The facies Gs display normally graded bedding and inversely and normally graded compound rhythms (Figs. 7e, 11d). These facies are composed of muddy sandstones and silt- to fine-graded sandstones, with plant debris distributed on the tops (Figs. 7e, 11d), and they can be attributed to deposits of suspended low-density turbidity currents (Bouma, 1962; Liu L et al., 2017; Li et al., 2021).

5.1.2.4 Fan fringe

The proximal part of the fan fringe is composed of the facies Gps or Gs and Cas (Fig. 7k), and the distal part consists of the facies Sm (Fig. 12f), Ms (Fig. 12g), Gs, Rs and Cas.

The combination of sandy debris flows or sandy high-density turbidity currents in the lower part and a compound of muddy debris flows or low-density turbidity currents in the upper part in a single sand layer are visible in the core; they are vertically superimposed in multiple stages and separated by background mudstone, indicating hybrid events (Haughton et al., 2009; Yang T et al., 2019b, 2021). The hybrid event beds that appear on the fan fringe are attributed to the fluid transition that occurred during the transport process of the hyperpycnal flow along the slope (Haughton et al., 2009; Li et al., 2021; Liu et al., 2021). The fan fringe is mainly developed with double-layered hybrid event beds, including three lithofacies assemblages. (1) The lower H1 divisions are composed of facies Gps or Ms, with eroding bottom mudstone, and the upper H3 divisions are composed of facies Cas (Fig. 7k). (2) The bottom unit of the H1 divisions consists of the

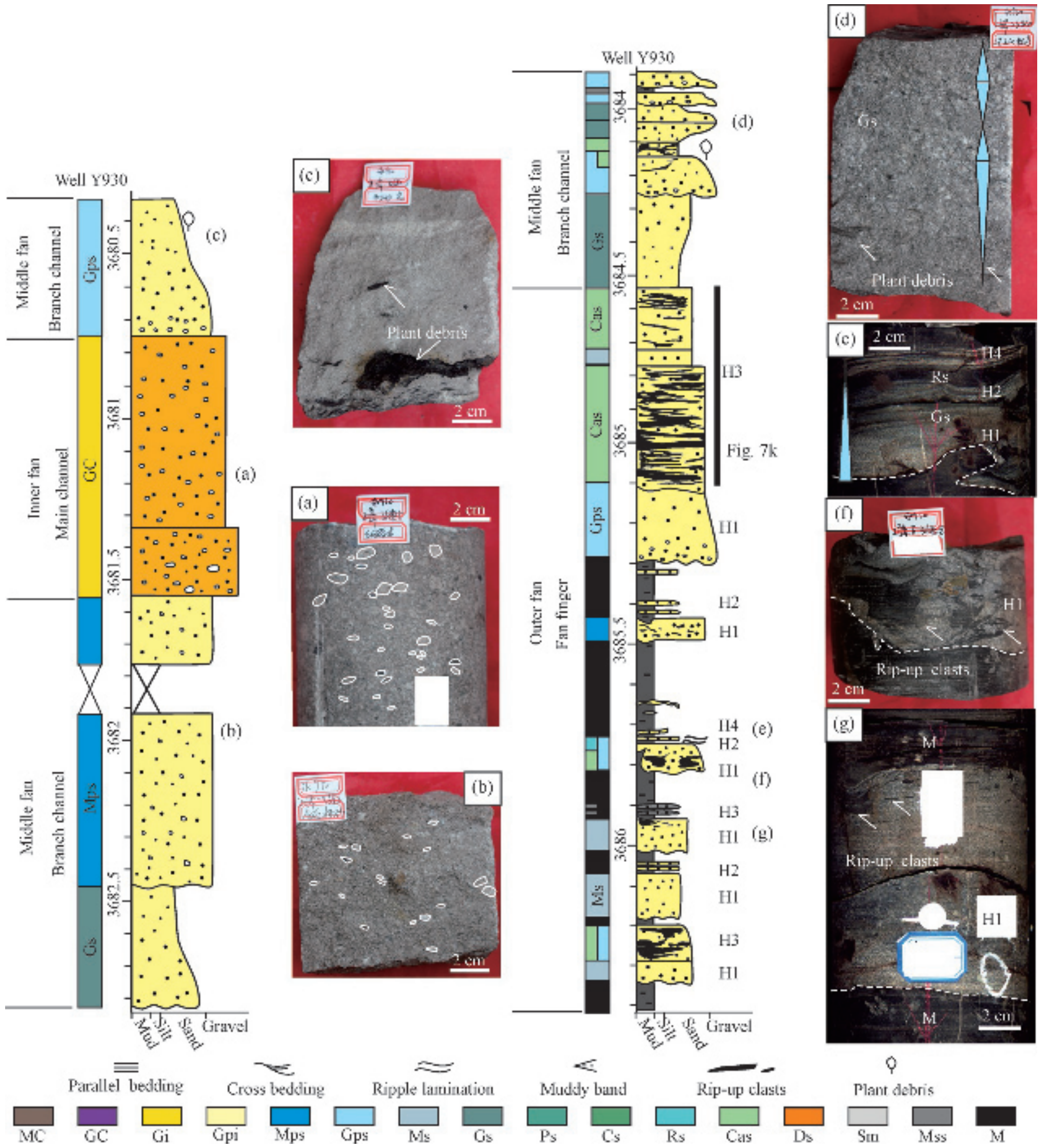

Fig. 12. Depositional characteristics of the late sublacustrine fan.

facies Ms, and the upper H2 divisions are composed of thin-bedded sandstone with mudstone. (3) The bottom unit of the H1 divisions comprises the facies Ms and erodes the basement mudstones, and the upper H3 divisions consist of mudstones interbedded with sandy mudstone strips. Hybrid event beds with a three-layer structure are also present: from base to top (H1), a lower coarser-grained layer containing muddy rip-up clasts and erosion of the base mudstone (Fig. 12f), (H2) a typically banded sandstone interbedded with mudstones, and (H4) a thin-bedded facies Rs.

5.2 Sedimentary processes and triggers analyses

Frequent fault activities and related earthquakes steepened the basin margin, formed large topographic drops, and increased sediment supply (Liu et al., 2021). The slope dips of the basin margin were 25.9°–34°, which were greater than the angle of repose of the coarse-grained sediments. During the early depositional period, thick-bedded gravelly debris flows (LA1) accumulated along the boundary fault, indicating abrupt strong energy (Fig. 13a, b).

During the early–middle deposition stage, the typical vertical sequences of the subaqueous fans developed in the western section (well Y928 area) and the eastern part (well Y936 area) displays fining-up grain size profiles. Furthermore, the vertical sequences are characterized at the bottom with the facies MC, which has a gravelly debris flow origin, and lacks the lower inversely graded part, suggesting extremely strong fluid energy; this energy is consistent with the description of the outburst-flood triggered hyperpycnal flow (Liu et al., 2021). The prograded subaqueous fans (similar to fan deltas) closer to

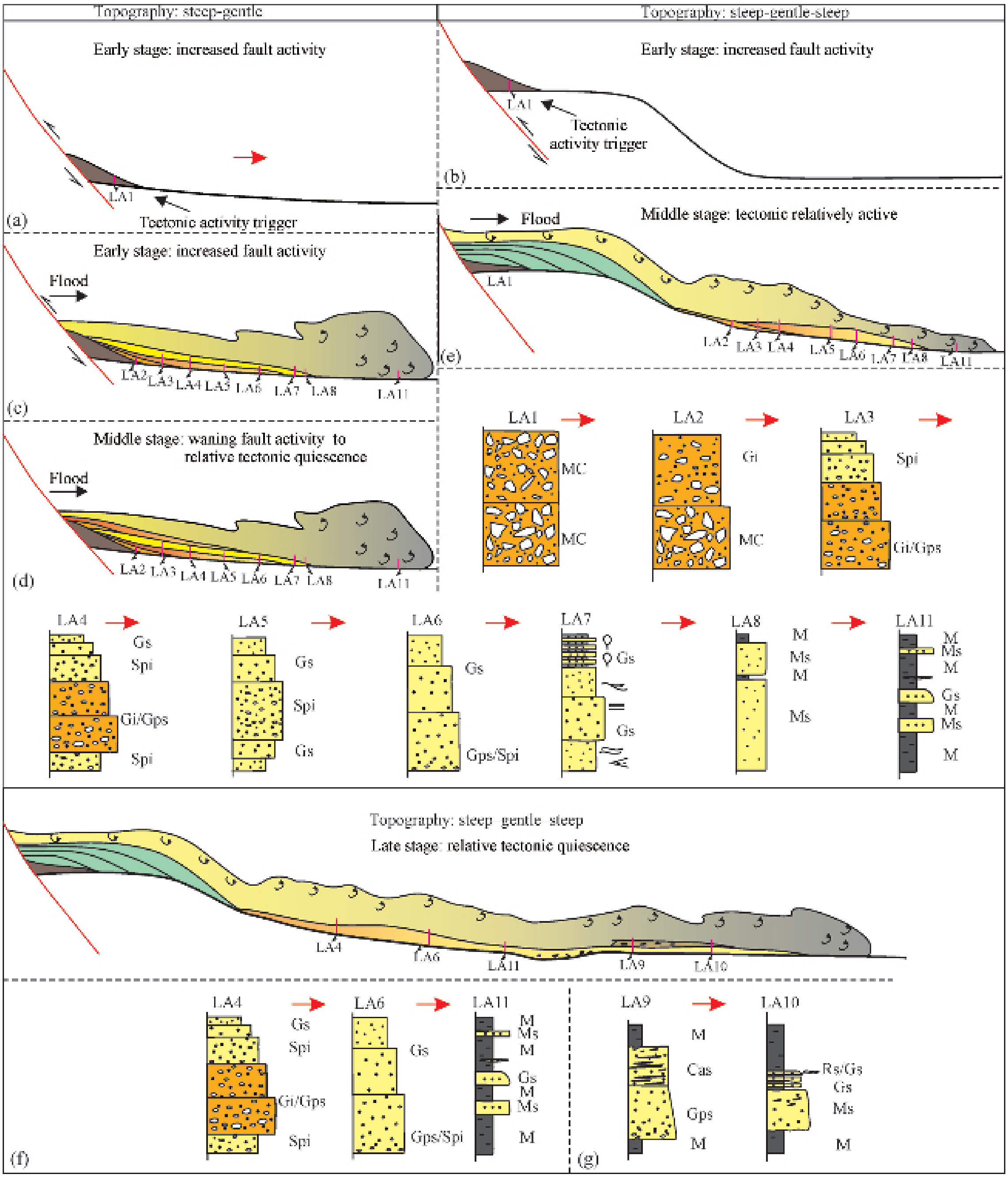

Fig. 13. Sedimentary mechanism of the coarse-grained subaqueous fans during the Es_4^{U-3} interval in the Yong′an area under different tectonic activities and geomorphological conditions.

the source (wells Y930, Y935 and Y933 areas) display vertical coarsening-upward sedimentary sequences, indicating more stable and sustained flood discharge, and the hyperpycnal flow caused by seasonal floods developed. The facies Gi, Cs and Rs appeared in the nearshore subaqueous fans, formed by the migration of bedforms from traction currents, and all typical lithofacies types appeared in hyperpycnal flows (Zavala et al., 2011). The bottom unit of the proximal hyperpycnal flow deposits is composed of the facies Gi, with overlying facies GC and Gs (LA3), which transformed into the bottom facies Gpi and overlying facies Gs (LA6) along the source direction. Finally, the distal part is dominated by mudstones interbedded with graded sandstone or massive sandstone. According to the lithofacies association evolution characteristics, seasonal flood-triggered hyperpycnal flows are composed of bedload gravelly traction currents and suspended gravelly high-density turbidity currents in the proximal part and transition to sandy traction currents with sandy high-density turbidity currents and finally to low-density turbidity currents at the end of the fan body (Fig. 13c–e).

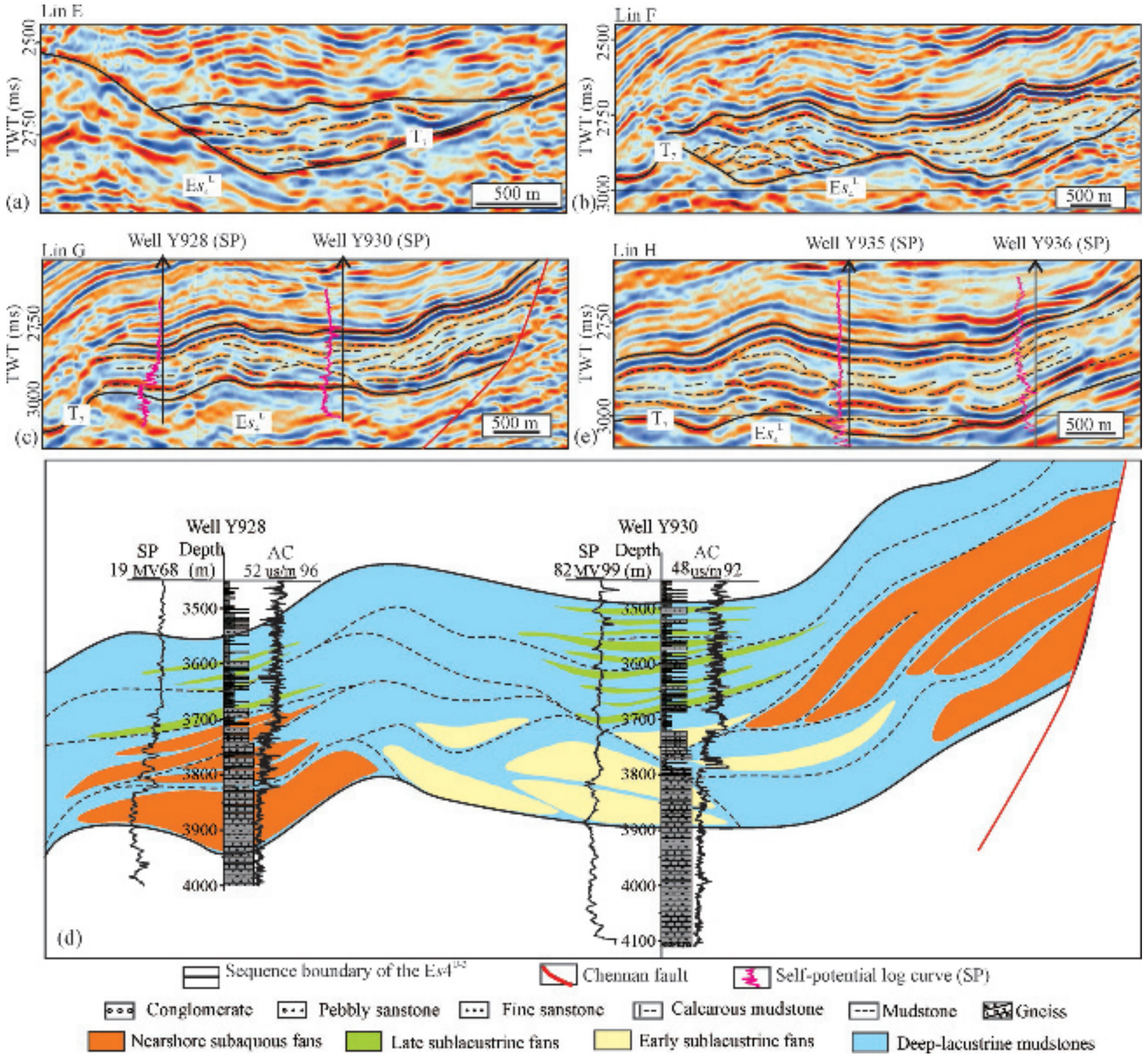

Fig. 14. Seismic profile perpendicular to the source direction (profile location is shown in Fig. 1e).

During the late deposition stage, the channel fills in the late sublacustrine fans generally display overall inverse to normal rhythms, indicating that the complete process of the initial increase and then decrease in flood energy is consistent with the previous description of flood gravity flows caused by seasonal floods (Fig. 13f) (Zavala et al., 2011). Debris flows, turbidity currents, transitional flows or hybrid event beds developed in the fan finger in late sublacustrine deposits (Fig. 13g). In the relatively proximal part, the sediments have coarse grain sizes, and the thickness of a single hybrid event bed is large. The lower H1 divisions consist of facies Gps or Ms, and the upper H3 divisions consist of facies Cas. The thickness of the lower unit of facies Cas (Fig. 7k), which is larger than that of the upper unit, may indicate relatively flat terrain and relatively weak tectonic activity, which are favorable for the development of the H3 divisions (Yang T et al., 2021). As the transport distance increases, the grain size of the sediments becomes finer, and the thickness of a single hybrid event bed decreases. In the relatively distal part, multiple stages of H1 interbedded with H2 or H3 divisions developed, separated by background mudstone, and the thickness of the lower H1 divisions is greater than that of the upper H2 or H3 divisions. As the transport distance increased and the fluid confinement weakened, it gradually transformed into a double-layer hybrid event bed caused by fluid expansion and deceleration, and the overall thickness of the mixing event layer decreased (Yang T et al., 2021).

5.3 Fault-activity dominated depositional model of steep belt in rift basin

5.3.1 Factors controlling the development of coarse-grained subaqueous fans

5.3.1.1 Paleotopography

The ancient gullies, which originated from the catchment regions and downcut the entire slope zone, are the provenance transport channels in the study area; they are steep upstream and gradually flatten downward (Sui et al., 2010; Zhang et al., 2019). The cross-sectional shape in the proximal end of the gully is V-shaped (Fig. 14a), with an internal seismic reflection of moderate amplitude intensity and poor lateral continuity. The cross-sectional shape evolves along the source direction into a nearly symmetrical W shape (Fig. 14b). The left gully (wells Y928–Y930 area) presents short-axis or intermittent seismic reflections, with lateral migration stacking. In contrast, the right gullies (wells Y930–Y936 area) are represented by continuous seismic reflectors and have an aggradational superposition in the vertical direction. The distal part of the gully (Fig. 14c, d) has an asymmetrical W shape in the strike direction, with continuous seismic reflectors. The width-to-depth ratio of the gullies increases from proximal to distal, reflecting a decrease in the erosive ability of the drainage system (Yang et al., 2019a).

The syn-sedimentary fault paleogeomorphic style in the study area developed fault scarp-type slope break belts, which are all steep boundary faults connected with a gentle basement; the steep slope dips of the boundary fault slopes are 25.9°–34° (Fig. 5; Table 2). The topographic changes in the western section (well Y928 area) and the eastern section (well Y936 area) both shift from steep to gentle along the source direction (Fig. 5a, d). The topographic change in the middle section (wells Y935 and Y930 areas) transitions from steeply to gently dipping and then dips steeply (Fig. 5b, c).

5.3.1.2 Paleoclimate

The sporopollen assemblage and geochemical analysis indicate that the mid-subtropical arid climate dominates the studied interval (Fig. 2) (Haughton et al., 2009; Li et al., 2021; Liu et al., 2021). The pollen species consist of high pollen Quercoidites of heat-loving subtropical plants. Compared with the Es_4^L, the Quercus content is much higher in Es_4^U, indicating a warm and humid environment, and the content of drought-tolerant Ephedra is reduced to 10% (Yao et al., 1994; He et al., 2007). The Sr/Cu and Mg/Ca ratios, with averages of 24.22 and 0.17, respectively, are relatively high, indicating an arid climate, and high oxygen isotope values indicate that evaporation is more significant than rainfall (Liu, 1998; Qian et al., 2009).

Table 2 Calculation of the dip angle of boundary faults

Measured line	Longitude (E)	Latitude (N)	TWT (ms)	Distance (m)	Elevation difference (m)	D_B (°)	tanD_B
Lin A	118.64° 118.64°	37.58° 37.59°	2996 2704	1075	522.01	25.90	0.49
Lin B	119.65° 119.65°	37.59° 37.60°	2886 2646	625	420.98	33.96	0.67
Lin C	119.66° 119.65°	37.59° 37.60°	2872 2598	834.42	477.23	29.77	0.57
Lin D	119.67° 119.67°	37.59° 37.59°	2930 2686	875	432.10	26.28	0.49
Lin E	119.68° 119.68°	37.57° 37.58°	2850 2498	1063.60	604.49	29.61	0.57

Note: D_B is the dip angle of boundary fault.

5.3.1.3 Parent rock characteristics

The skeletal composition of the clastic rocks shows the most direct evidence of the source rock properties and the tectonic background of the parent rock area (Dickinson and Suczek, 1979; Xia, 2019). Single minerals and rock fragments were identified using optical properties under transmitted light on a petrographic microscope. The framework grain types and contents of 112 thin sections were quantified by using the Dickinson-Gazzi thin section point count technique, and the findings are reported in Table 3. The Q/(F + R) ratios are all less than 1, indicating their low compositional maturity and their near-source rapid accumulation characteristics. The rock fragment contents show a decreasing trend, while the compositional maturity increases sequentially from the nearshore subaqueous fan to the early sublacustrine fan and then to the late sublacustrine fan.

According to the discriminant function diagram of the major elements (McLennan et al., 1993) (Fig. 15a) and the La/Th-Hf and Co/Th-La/Sc source rock discriminant diagrams (Fig. 15b, c), the parent rock is mainly derived from intermediate-acid igneous rocks and intermediate-basic igneous rocks (Chen, 2020). Intermediate-acid igneous rocks under dry climate conditions are subject to weak chemical weathering (Xia, 2019).

The average content of metamorphic rock fragments is 13.71%, followed by sedimentary rock fragments, with

Table 3 Composition of rock fragment types during the E$s_4^{U\text{-}3}$ interval

Genetic types	Nearshore subaqueous fan				Early sublacustrine fan			Late sublacustrine fan			
Well	Y928	Y933	Y936	Average	Y930	Y935	Average	Y928	Y930	Y936	Average
Quartz	27.49%	32.83%	31.94%	30.75%	33.10%	33.41%	33.25%	35.06%	32.34%	38.91%	35.44%
Feldspar	45.60%	51.12%	50.62%	49.12%	51.01%	50.54%	50.78%	50.51%	53.21%	46.89%	50.20%
Total rock fragment	25.21%	16.05%	15.04%	18.77%	13.20%	12.59%	12.90%	9.50%	11.91%	10.33%	10.58%
Q/(F + R)	0.39	0.49	0.49	0.45	0.52	0.53	0.52	0.58	0.50	0.68	0.58
Metamorphic rock fragment + igeous rock fragment	21.82%	13.94%	8.35%	14.70%	8.59%	6.42%	7.51%	4.84%	7.06%	5.21%	5.70%
Metamorphic rock fragment	19.53%	13.53%	8.06%	13.71%	8.40%	6.00%	7.20%	3.95%	6.80%	4.71%	5.15%
Quartzofeldspathic metamorphic rock fragment	18.39%	12.41%	6.81%	12.54%	5.03%	3.26%	4.14%	2.41%	4.52%	3.99%	3.64%
Metamorphic clay rock fragment	1.14%	1.03%	0.63%	0.93%	2.05%	2.71%	2.38%	1.43%	1.99%	0.67%	1.36%
Metamorphic rock fragment	0	0	0	0	1.32%	0.03%	0.68%	0.12%	0.05%	0	0.06%
Quartzite rock fragment	0	0.09%	0.04%	0.04%	0	0	0	0.00%	0.24%	0.05%	0.10%
Igeous rock fragment	2.29%	0.42%	0.29%	1.00%	0.19%	0.42%	0.31%	0.89%	0.26%	0.50%	0.55%
Sedimentary rock fragment	3.33%	1.93%	6.62%	3.96%	4.61%	6.17%	5.39%	4.66%	4.85%	5.08%	4.86%
Sandy rock fragment + siliceous rock fragment	0	0.32%	0.02%	0.11%	0	0.14%	0.07%	0	0	0	0
Carbonate rock fragment	3.33%	1.61%	6.60%	3.85%	4.61%	6.04%	5.32%	4.66%	4.85%	5.08%	4.86%

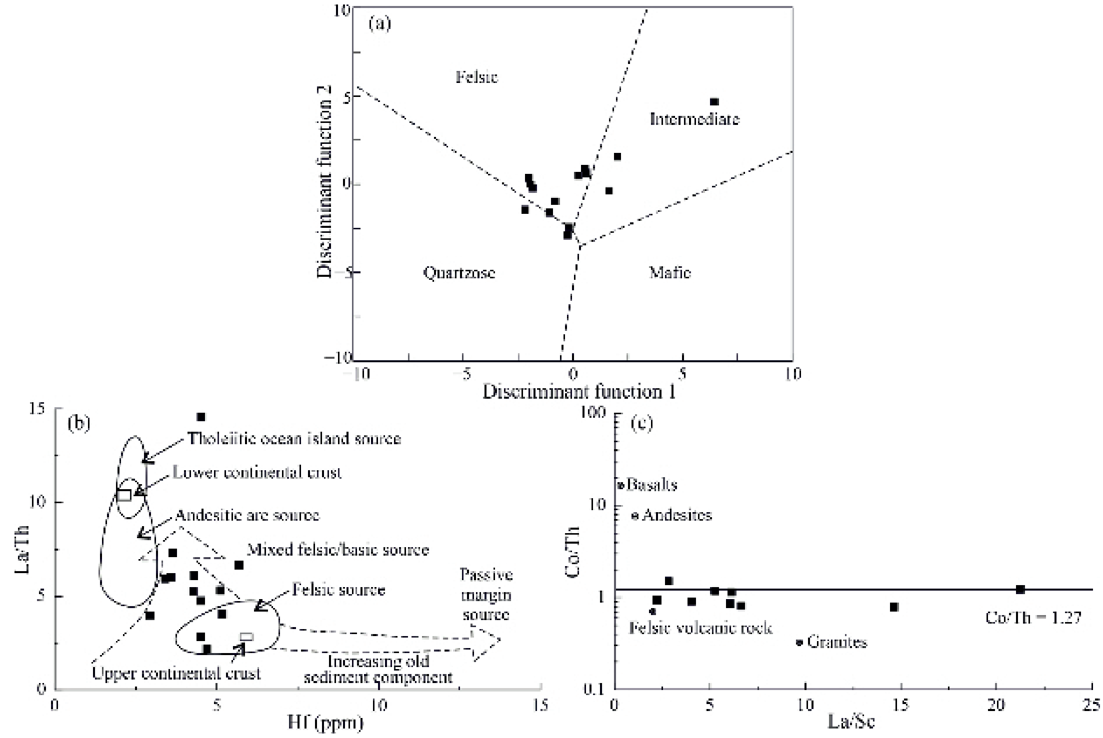

Fig. 15. Bivariate discrimination plots.
(a) Th/U vs. Th plot (after McLennan, 1993); (b) La/Th vs. Hf (after Floyd and Leveridge, 1987); (c) La/Sc vs. Co/Th (after Gu, 2002). The samples are mudstone and siltstone taken from the Es_4^U of wells Y935, Y930 and Y920. The datas are from Chen (2020).

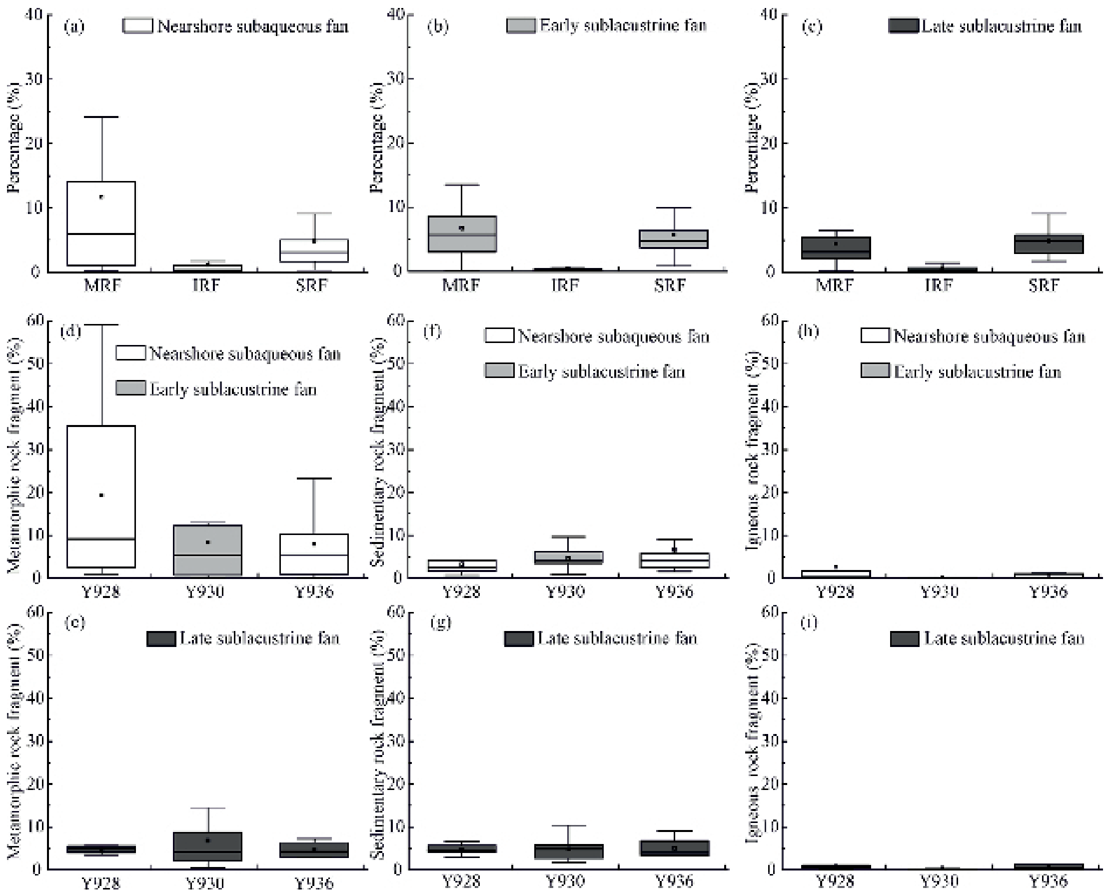

Fig. 16. Relative contents of rock fragment components of each sedimentary facies type.

an average of 3.96% (Fig. 16a). For the early sublacustrine fan, the average content of metamorphic rock fragments is 7.2%, which is slightly higher than that of sedimentary rock fragments (Fig. 16b). The average content of metamorphic rock fragments in the late sublacustrine fan is comparable to that of sedimentary rock fragments (Fig. 16c). The felsic metamorphic rock fragments dominate the metamorphic rock fragments, and the sedimentary rock fragments are dominated by carbonate rock fragments (Table 3). A comparison of the variations in different rock fragment types in wells Y928, Y930 and Y936 reveals that the average content of metamorphic rock fragments in the early fans is higher than that in the late fans (Fig. 16d–i). Strong tectonic uplift and earthquake-triggered landslides can lead to extremely strong physical erosion (Dadson et al., 2003; Kao and Milliman, 2008), and the high content of metamorphic rock fragments in the early fans indicates early active tectonic movement. During the late depositional stage of the target interval, the sum of the average contents of metamorphic and igneous rock fragments in wells Y928 and Y936 was slightly higher than that of sedimentary rock fragments, while the contents of metamorphic and igneous rock fragments in well Y930 were significantly higher (Table 3; Fig. 16e, g, i). A comparison of the internal architectures of the coarse-grained sediments in the three regions reveals that the supply system of the late sublacustrine fan is different among the three regions. The sublacustrine fan in the middle section (well Y930 area) was supplied by a prograded fan, indicating that its sediment supply rate was greater than the increased rate of the accommodation space. The sublacustrine fans in the eastern section (well Y936 area) and the western section (well Y928 area) were supplied by a retrograded fan during the late stage. However, the intensity of tectonic activity in the middle section of the study area (well Y930 area) is lower than that in the western section (well Y928 area) and the eastern section (well Y936 area). Furthermore, the contents of metamorphic rock fragments and igneous rock fragments in well Y930 are significantly higher, which may indicate that geomorphology affected the supply of coarse-grained sediments.

5.3.2 Depositional model of the coarse-grained subaqueous fans

At the beginning of deposition in the study interval, increased fault activity formed new accommodation space, increased sediment supply, and increased the thickness and scale of the sedimentary strata (Li et al., 2021). The wedge -shaped seismic reflection facies are related to the tectonic activity developed in the slope break belts (Fig. 17a, b). Close to the boundary fault, the thickness of the clastic wedge gradually decreases. The clastic wedge deposits connected the steep boundary fault and the gentle basement, and formed new transport channels.

Long-lived seasonal flooding in relatively arid climates is ideal for hyperpycnal flow development (Mulder et al., 2003; Petter and Steel, 2006; Yang et al., 2015). During the middle deposition stage, floods carried a large amount of coarse-grained clastic deposits into the deep lake by the slope face of the wedge. The ratio between the rate of accommodation space increased and the rate of sediment supply controlled the vertical stacking pattern of the coarse-grained sediments. In addition to tectonic factors, flood discharge intensity impacts sediment filling (Chen et al., 2019; Yang et al., 2022). In the middle section (wells Y930 and Y935 area), the drainage systems carried coarse-grained sediment into the catchment areas by the relatively gentle relay ramps. With a relatively small intensity of tectonic activity and more stable and sustained flood discharge, prograded subaqueous fans developed (Fig. 17c). In contrast, the western (well Y928 area) and eastern (well Y936 area) sections had stronger tectonic activity and large topographic drops, which continued to generate new accommodation space, and retrograded subaqueous fans developed, corresponding to bell-shaped SP log curves (Figs. 5a, b, 17d). The mid-subtropical arid climate also prompted the development of distal sublacustrine fans (Liu et al., 2021). The topography of the middle section shows a gentle to steep trend along the source direction, and floods carried terrigenous sediments continued into deep waters along a second-order steep slope. The early retrograded sublacustrine fan developed at the fronts of the nearshore subaqueous fans, which had considerable thicknesses and corresponded to funnel-shaped SP logging curves (Figs. 5b, c, 8a, b, 17c). During the period of waning fault activity to relative tectonic quiescence, with the continuous and stable supply of floods, flood-triggered hyperpycnal flows developed. During the late deposition stage, late sublacustrine fans transpoted by hyperpycnal flows developed in the deep lake environment, and their seismic reflection were lenticular, with multiple stages superimposed on the plane (Figs. 8, 17e, f).

6 Conclusions

The genetic types of the coarse-grained subaqueous fans in the study area include nearshore subaqueous fans, early sublacustrine fans and late sublacustrine fans. The seismic reflection of the nearshore subaqueous fans is characterized by the development of wedge-shaped reflection facies at the bottom and the development of retrograded seismic facies or prograded seismic facies at the top, both of which are in angular unconformity contact. The early sublacustrine fan developed retrograded seismic facies, and the late sublacustrine fan developed lenticular reflection facies.

Frequent fault activity and related earthquakes steepened the basin margin, and the boundary fault slopes were 25.9°–34°. The coarse-grained sediments were transported by gravity and formed a thick-bedded superimposed conglomerate of debris flow origin along the boundary fault. During the early–middle deposition stage, outburst floods associated with tectonic activity triggered hyperpycnal flows developed. The sedimentary sequence is characterized by thick conglomerates of debris flows originating at the bottom, lacking the lower coarsening-upward grain size portion. During the late deposition stage of weak tectonic activity, seasonal floods triggered hyperpycnal flows with hybrid event beds that developed at the distal part.

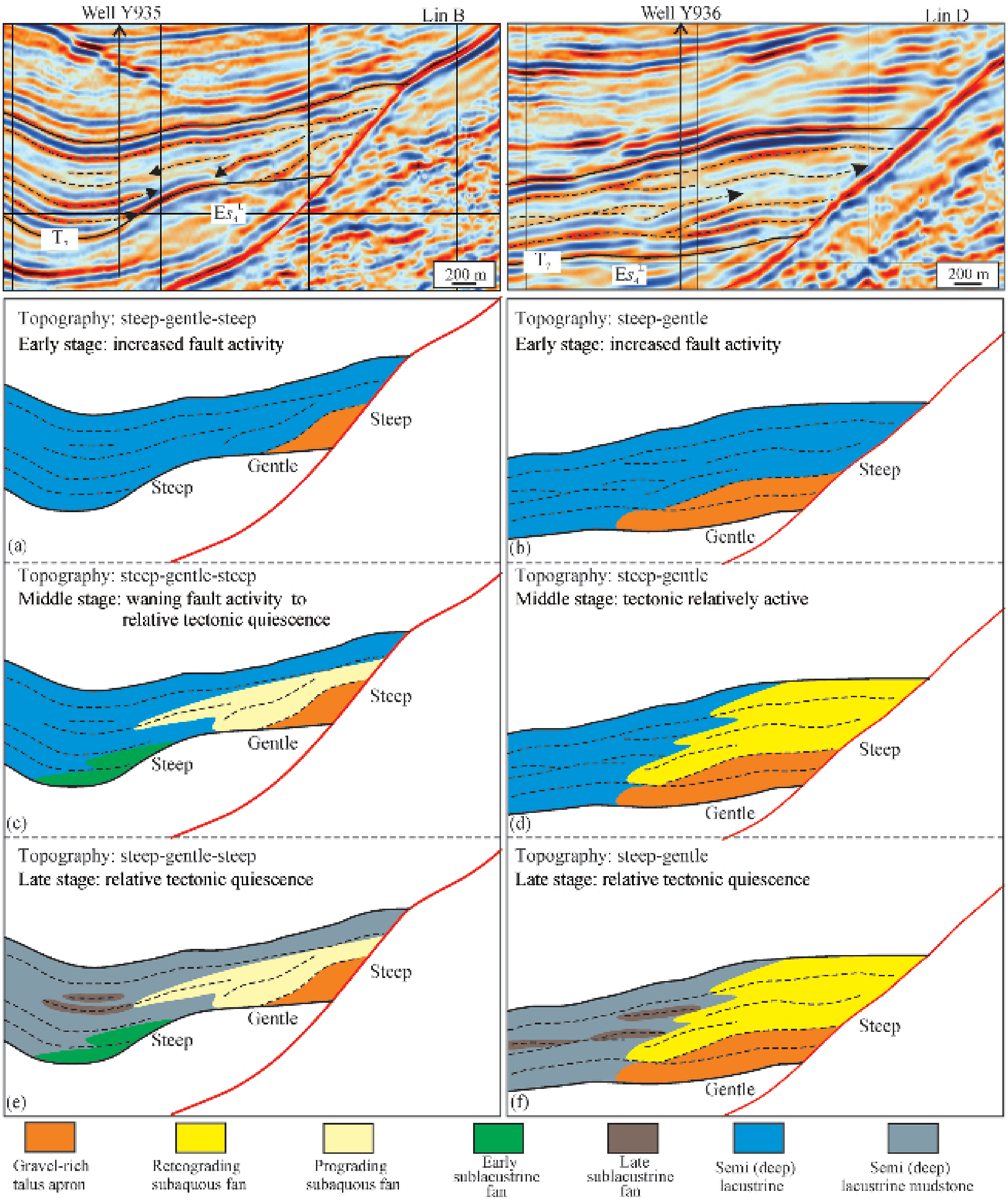

Fig. 17. Depositional model of coarse-grained subaqueous fans during the $Es_4^{U\text{-}3}$ interval in the Yong'an area, Dongying Depression.

The sedimentary process, deposition pattern and distribution of the subaqueous fans in the study area were mainly controlled by tectonic activity and paleogeomorphology. During the early–middle deposition stage, nearshore subaqueous fans developed close to the boundary faults, with active tectonics and large topographic drops. In the middle section of the study area, the topography changed from gentle to steep along the source direction, and the early sublacustrine fan developed at the front of the nearshore subaqueous fans, displaying a retrograding superimposition with a large thickness. In the eastern and western sections, the topography of the deep lake area was relatively flat, and no sublacustrine fans developed. During the late deposition stage, with weak tectonic activity, late distal sublacustrine fans developed in the deep lake environment, and their seismic reflections were lenticular, with multiple stages superimposed on the plane.

Acknowledgments

This study is supported by the National Science

Foundation of China (Grant Nos. 41972099, 4217020246), the National Science and Technology Major of China (Grant Nos. 2017ZX05009-002, 2017ZX05072-002). We want to thank the Shengli Oilfield, SINOPEC, for providing original data and permission to publish this article. We also thank to the editors and two anonymous reviewers for providing valuable comments and advice that significantly improved the quality of this paper.

Manuscript received May 10, 2022
accepted Jul. 13, 2022
associate EIC: JIAN Zhimin
edited by GUO Xianqing

References

Bouma, A.H., and Shepard, F.P., 1962. Sedimentology of Some Flysch Deposits; A Graphic Approach to Facies Interpretation. Amsterdam: Elsevier Publishing Company, 1–168.

Cao, Y.C., Wang, Y.Z., Gluyas, J.G., Liu, H.M., Liu, H.N., Song, M.S., and Marzo, M., 2018. Depositional model for lacustrine nearshore subaqueous fans in a rift basin: The Eocene Shahejie Formation, Dongying Sag, Bohai Bay Basin, China. Sedimentology, 65: 2117–2148.

Chen, L., Ji, H.C., Zhang, L., Zhu, Y., Fang, Z., and Patacci, M., 2019. Rift activity and sequence stratigraphy of the Oligocene Dongying Formation in the Nanpu Sag, eastern China: Implications for rift sequence stratigraphy in lacustrine basins. Geological Journal, 55: 1163–1178.

Chen, S.R., 2020. Comparative Study of Glutenite Reservoir Differences of the E*s*4s in the Yanjia-Yong'an Block of the Northern Zone of Dongying Depression (M.Sc. thesis). Qingdao: China University of Petroleum (East China), 19–28 (in Chinese with English abstract).

Chiarella, D., Capella, W., Longhitano, S.G., and Muto, F., 2021. Fault-controlled base-of-scarp deposits. Basin Research, 33: 1056–1075.

Dadson, S.J., Hovius, N., Chen, H.G., Dade, W.B., Hsieh, M.L., Willett, S.D., Hu, J.C., Horng, M.J., Chen, M.C., Stark, C.P., Lague, D., and Lin, J.C., 2003. Links between erosion, runoff variability and seismicity in the Taiwan orogen. Nature, 426: 648–651.

Deng, H.W., Wang, H.L., and Wang, D.Z., 2001. Control of Paleo-Morphology to stratigraphic sequence in continental rift basins: Take Lower Tertiary of western slope in Bozhong depression as an example. Oil & Gas Geology, 22: 293–296 (in Chinese with English abstract).

Dickinson, W.R., and Suczek, C.A., 1979. Plate tectonics and sandstone compositions. AAPG Bulletin, 63: 2164–2182.

Dong, D.T., Qiu, L.W., Ma, Y.D., Yang, Y.Q., Zou, Y., Dai, L., Teng, B.G., and Zhang, Z.P., 2018. Control of tectonics on sedimentation of sandstone and process of sedimentfilling in multi-fault lacustrine basins: A case study on the Eocene ineastern Zhanhua Sag, Jiyang Depression in Bohai Bay Basin. Oil & Gas Geology, 39(4): 653–663 (in Chinese with English abstract).

Dong, D.T., Qiu, L.W., Ma, P.J., Yu, G.D., Wang, Y.Z, Zhou, S.B., Yang, B.L., Huang, H.Q., Yang, Y.Q., and Li, X., 2022. Initiation and evolution of coarse-grained deposits in the Late Quaternary Lake Chenghai source-to-sink system: From subaqueous colluvial apron (subaqueous fans) to Gilbert-type delta. Journal of Palaeogeography, 11(2): 14–221.

Dong, G.Y., and He, Y.B., 2016. Mechanism of sand body predictioninacontinentalrift basin by coupling paleogeomorphic elements under the control of base level. Petroleum Exploration and Development, 43(4): 529–539.

Feng, Y.L., 1999. Lower tertiary stratigraphic framework and basing filling model in Dongying depression. Earth Science, 24(6): 635–642 (in Chinese with English abstract).

Feng, Y.L., 2006. Control of valley and tectonic slope break zone on sand bodies in rift-subsidence basin. Acta Petrolei Sinica, 27(1): 13–16 (in Chinese with English abstract).

Feng, Y.L., Li, S.T., and Lu, Y.C., 2013. Sequence stratigraphy and architectural variability in Late Eocene lacustrine strata of the Dongying Depression, Bohai Bay Basin, Eastern China. Sedimentary Geology, 295: 1–26.

Floyd, P.A., and Leveridge, B.E., 1987. Tectonic environment of the Devonian Gramscatho basin, south Cornwall: Framework mode and geochemical evidence from turbiditic sandstones. Journal of the Geological Society, 144(4): 531–542.

Galloway, W.E., 1998. Siliciclastic slope and base-of-slope depositional systems: Component facies, stratigraphic architecture, and classification. AAPG Bulletin, 82: 569–595.

Gu, X.X., Liu, J.M., Zheng, M.H., Tang, J.X., and Qi, L., 2002. Provenance and tectonic setting of the Proterozoic turbidites in Hunan, South China: Geochemical evidence. Journal of Sedimentary Research, 72: 393–407.

Haughton, P., Davis, C., McCaffrey, W., and Barker, S., 2009. Hybrid sediment gravity flow deposits—Classification, origin and significance. Marine and Petroleum Geology, 26: 1900–1918.

He, Z.J., Jiang, G.X., Jia, F.H., Bian, X.M., and Wei, W.Y., 2007. The paleogene palynology and sequence stratigraphy in the Jiyang depression. Journal of Stratigraphy, 31(4): 407–414 (in Chinese with English abstract).

Henstra, G.A., Grundvåg, S.A., Johannessen, E.P., Kristensen, T.B., Midtkandal, I., Nystuen, J.P., Rotevatn, A., Surlyk, F., Sæther, T., and Windelstad, J., 2016. Depositional processes and stratigraphic architecture within a coarse-grained rift-margin turbidite system: The Wollaston Forland Group, east Greenland. Marine and Petroleum Geology, 76: 187–209.

Hu, S.B., O'Sullivan, P.B., Raza, A., and Kohn, B.P., 2001. Thermal history and tectonic subsidence of the Bohai Basin, northern China: A Cenozoic rifted and local pull-apart basin. Physics of the Earth and Planetary Interiors, 126: 221–235.

Kao, S.J., and Milliman, J.D., 2008. Water and sediment discharge from Small Mountainous Rivers, Taiwan: The roles of lithology, episodic events, and human activities. The Journal of Geology, 116: 431–448.

Legros, F., 2002. Can dispersive pressure cause inverse grading in grain flows? Journal of Sedimentary Research, 72(1): 166–170.

Li, J., Liu, Z., Liu, J.P., Chen, L., Liu, H.M., Huang, L.L., Qian, L.L., Lu, K., and Liu, K.M., 2021. Transformation of sediment delivery and dispersal patterns controlled by relay-ramp evolution along the boundary fault of a lacustrine rift: The Eocene Shahejie formation, Dongying Sag, Bohai Bay Basin, NE China. Marine and Petroleum Geology, 128: 105044.

Li, Z.X., Yang, W., Wang, Y.S., Zhang, L.Q., Luo, H.M., Liu, S.H., Zhang, L.K., and Luo, X.R., 2019. Anatomy of a lacustrine stratigraphic sequence within the fourth member of the Eocene Shahejie Formation along the steep margin of the Dongying depression, eastern China. AAPG Bulletin, 103: 469–504.

Lin, C.S., 2004. The control of syndepositional faulting on the Eogene sedimentary basin fills of the Dongying and Zhanhua sags, Bohai Bay Basin. Science in China Series D: Earth Sciences, 47(9): 769–782.

Liu, C.L., 1998. Carbon and oxygen isotopic compositions of lacustrine carbonates of the Shahejie formation in the Dongying depression and their paleolimnological significance. Acta Sedimentologica Sinica, 16: 109–114 (in Chinese with English abstract).

Liu, H., Loon, A.J., Xu, J., Tian, L.X., Du, X.F., Zhang, X.T., and Chen, D.L., 2019. Relationships between tectonic activity and sedimentary source-to-sink system parameters in a lacustrine rift basin: A quantitative case study of the Huanghekou Depression (Bohai Bay Basin, E China). Basin Research, 32 (4): 587–612.

Liu, J.P., Xian, B.Z., Wang, J.H., Ji, Y.L., Lu, Z.Y., and Liu, S.J., 2017. Sedimentary architecture of a sub-lacustrine debris fan: Eocene Dongying Depression, Bohai Bay Basin, east China. Sedimentary Geology, 362: 66–82.

Liu, L., Chen, H.D., Wen, H.G., Xu, W.L., Zhong, Y.J., Wang, X.L., and Wang, Z.W., 2020. Facies architecture and sediment infilling processes in intrabasinal slope belts of lacustrine rift basins, Zhanhua Depression, Bohai Bay Basin. Marine and Petroleum Geology, 112: 104089.

Liu, J.P., Xian, B.Z., Tan, X.F., Zhang, L., Su, M., Wu, Q.R., Wang, Z., Chen, P., He, Y.X., Zhang, S.H., Li, J., Gao, Y., and Yu, Q.H., 2021. Depositional process and dispersal pattern of a faulted margin hyperpycnal system: The Eocene Dongying depression, Bohai bay basin, China. Marine and Petroleum Geology, 135: 105405.
Liu, L., Chen, H.D., Zhong, Y.J., Wang, J., Xu, C.G., Chen, A.Q., and Du, X.F., 2017. Sedimentological characteristics and depositional processes of sediment gravity flows in rift basins: The Palaeogene Dongying and Shahejie formations, Bohai Bay Basin, China. Journal of Asian Earth Sciences, 147: 60–78.
Liu, Q.H., Zhu, H.T., Du, X.F., Xue, Y.A., Yang, X.H., Yang, H.F., Shi, W.L., and Zhou, Z.Q., 2020. Development and hotspot of sedimentary response of glutenite in the offshore Bohai Bay Basin. Earth Science, 45: 1676–1705 (in Chinese with English abstract).
Lowe, D.R., 1976. Grain flow and grain flow deposits. Journal of Sedimentary Research, 46: 188–199.
Lowe, D.R., 1982. Sediment gravity flows; II, Depositional models with special reference to the deposits of high-density turbidity currents. Journal of Sedimentary Research, 52: 279–297.
Ma, B.B., Eriksson, K.A., Cao, Y.C., Jia, Y.C., Wang, Y.Z., and Gill, B.C., 2016. Fluid flow and related diagenetic processes in a rift basin: Evidence from the fourth member of the Eocene Shahejie Formation interval, Dongying depression, Bohai Bay Basin, China. AAPG Bulletin, 100(11): 1633–1662.
Ma, P.J., Lin, C.Y., Ren, L.H., Jahren, J., Dong, D.T., Yu, G.D., Ma, C.F., Wang, D., Liu, L.Q., and Hellevang, H., 2021. Linkage and growth of the independent and coherent faults: Insight into the effect of relay ramps on sedimentation patterns in the northern Bonan Sag, Bohai Bay Basin. Marine and Petroleum Geology, 127: 104985.
Martins-Neto, M.A., and Catuneanu O., 2010. Rift sequence stratigraphy. Marine and Petroleum Geology, 27: 247–253.
McLennan, S.M., Hemming, S., McDaniel, D.K., and Hanson, G.N., 1993. Geochemical approaches to sedimentation, provenance, and tectonics. In: Johnsson, M.J., and Basu, A. (eds.), Processes Controlling the Composition of Clastic Sediments. Geological Society of America, 284: 21–40.
Mulder, T., Syvitski, J.P.M., Migeon, S., Faugères, J.C., and Savoye, B., 2003. Marine hyperpycnal flows: initiation, behavior and related deposits. A review. Marine and Petroleum Geology, 20: 861–882.
Nemec, S., 1990. Aspects of sediment movement on steep delta slopes. In: Colella, A., and Prior, D.B. (eds.), Coarse-Grained Deltas. Special Publications of the International Association of Sedimentologists, 10: 29–74.
Petter, A.L., and Steel, R.J., 2006. Hyperpycnal flow variability and slope organization on an Eocene shelf margin, Central Basin, Spitsbergen. AAPG Bulletin, 90: 1451–1472.
Posamentier, H.W., and Kolla, V., 2003. Seismic geomorphology and stratigraphy of depositional elements in deep-water settings. Journal of Sedimentary Research, 73: 367–388.
Qian, H.J., Lu, X.C., Zhang, X.F., Zhang, L.Y., and Liu, Q., 2009. Spatial paleosalinity distribution and element geochemistry of Argil-Laceous source rocks in the upper part of 4th member of Tertiary Shahejie formation in Dongying sag. Acta Petrologica et Mineralogica, 28(2): 161–168 (in Chinese with English abstract).
Shang, W.L., Xu, S.H., Mao, Z.Q., Li, X.G., Gao, G., Li, Z.Y., and Qin, L., 2022. High-resolution sequence stratigraphy in continental lacustrine basin: A case of Eocene Shahejie Formation in the Dongying Depression, Bohai Bay Basin. Marine and Petroleum Geology, 136: 105438.
Shanmugam, G., 2012. New perspectives on deep-water sandstones: Origin, recognition, initiation and reservoir quality. Handbook of Petroleum Exploration and Production, 9: 524.
Sohn, Y.K., 1997. On traction-carpet sedimentation. Journal of Sedimentary Research, 67: 502–509.
Song, M.S., 2018. The exploration status and outlook of Jiyang depression. China Petroleum Exploration, 23(3): 11–17 (in Chinese with English abstract).
Sui, F.G., Cao, Y.C., Liu, H.M., and Wang, Y.Z., 2010. Physical properties evolution and hydrocarbon accumulation of Paleogene nearshore subaqueous fan in the eastern north margin of the Dongying depression. Acta Geologica Sinica, 84 (2): 246–256 (in Chinese with English abstract).
Surlyk, F., 1984. Fan-delta to submarine fan conglomerates of the Volgian-Valanginian Wollaston Foreland Group, East Greenland. In: Koster, E.H., and Steel, R.J. (eds.), Sedimentology of Gravels and Conglomerates. Canadian Society of Petroleum Geologists, Memoir, 10: 359–382.
Talling, P.J., Masson, D.G., Sumner, E.J., and Malgesini, G., 2012. Subaqueous sediment density flows: Depositional processes and deposit types. Sedimentology, 59(7): 1937–2003.
Wang, Y.S., 2021. Ideas and directions for oil and gas exploration in different fields of Jiyang Depression, Bohai Bay Basin, China. Petroleum Geology and Recovery Efficiency, 28(5): 28–36 (in Chinese with English abstract).
Wang, Y.M., Jin, W.D., Liu, S.H., Qiu, G.Q., Li, Q., Li, H., Xin, R.C., and Yang, F., 2003. Genetic types,distribution and exploration significance of multistage slope breaks in rift Lacustrine Basin genetic types. Oil & Gas Geology, 24(3): 199–203 (in Chinese with English abstract).
Wang, Y.S., Wang, Y., Zhu, D.S., Ding, J.H., Shang, B., and Zhu, J.J., 2016. Genetic mechanism of high-quality glutenite reservoirs at the steep slope in northern Dongying sag. China Petroleum Exploration, 21: 28–36 (in Chinese with English abstract).
Xia, F.Y., 2019. Comprehensive provenance study and tectonic setting of sandstones from the upper Cretaceous Yaojia Formation, Qianjiadian area, southern Songliao basin (Ph.D. thesis). Wuhan: China University of Geosciences, 67–68 (in Chinese with English abstract).
Xian, B.Z., Wang, Y.S., Zhou, T.Q., and Sun, L.D., 2007. Distribution and controlling factors of glutinite bodies in the actic region of a rift basin: An example from Chezhen Sag, Bohai Bay Basin. Petroleum Exploration and Development, 34(4): 429–436 (in Chinese with English abstract).
Yang, B.L., Qiu, L.W., Yang, Y.Q., Dong, D.T., Zhou, S.B., Liu, Z.W., and Bai, L.K., 2021. Sedimentary characteristics and transport mechanism of subaqueous coarse clastic rocks in the lower Cretaceous xiguayuan formation in the steep slope zone of Luanping basin. Earth Science, 46(9): 3258–3277 (in Chinese with English abstract).
Yang, B.L., Qiu, L.W., Yang, Y.Q., Wang, Y.L., Nan, J.M., Xu, N.N., Xu, S., and Zhang, H.F., 2022. Sediment transport mechanism and development characteristics of subaqueous fan in the northern steep slope zone of Lijin sag. Journal of China University of Petroleum (Edition of Natural Science), 46(2): 25–37 (in Chinese with English abstract).
Yang, T., Cao, Y.C., Wang, Y.Z., Zhang, S.M., Zhang, H.N., and Wang, S.J., 2015. Sediment dynamics process and sedimentary characteristics of hyperpycnal flows. Geological Review, 61(1): 23–33 (in Chinese with English abstract).
Yang, T., Cao, Y.C., Liu, K.Y., Wang, Y.Z., Zavala, C., Friis, H., Song, M.S., Yuan, G.H., Liang, C., Xi, K.L., and Wang, J., 2019a. Genesis and depositional model of subaqueous sediment gravity-flow deposits in a lacustrine rift basin as exemplified by the Eocene Shahejie Formation in the Jiyang Depression, Eastern China. Marine and Petroleum Geology, 102: 231–257.
Yang, T., Cao, Y.C., Liu, K.Y., Zhou, L.L., and Jin, J.H., 2019b. Origin of deep-water fine-grained sediments as revealed from the Lower Cretaceous rifting basin sequence in the Lingshan Island, Yellow Sea, Eastern China. Journal of Asian Earth Sciences, 186: 104065.
Yang, T., Cao, Y.C., Tian, J.C., Niu, X.B., Li, S.X., Zhou, X.P., Jin, J.H., and Zhang, Y.A., 2021. Deposition of deep-water gravity-flow hybrid event beds in lacustrine basins and their sedimentological significance. Acta Geologica Sinica, 95(12): 3842–3857 (in Chinese with English abstract).
Yao, Y.M., Lian, H.D., and Cai, Z.G., 1994. Tertiary in Petroliferous Regions of China (IV): The Bohai Gulf Basin. Beijing: Petroleum Industry Press, 55–57 (in Chinese).

Yu, J.F., Liu, T.J., Jia, H.B., Jiang, Z.H., Wei, S.H., Li, Y.P., and Ma, S.B., 2021. Controlling factors analyses of sediment dispersal from source-to-sink systems of lacustrine rift basin: A case study from Paleogene Shahejie–Dongying formations of Nanpu Sag, eastern China. Frontiers in Earth Science, 9: 716176.

Zavala, C., Arcuri, M., Di Meglio, M., Gamero, H., and Contreras, C., 2011. A genetic facies tract for the analysis of sustained hyperpycnal flow deposits. In: Slatt, R.M., and Zavala, C. (eds.), Sediment Transfer from Shelf to Deep Water—Revisiting the Delivery System. American Association of Petroleum Geologists, 31–51.

Zavala, C., 2020. Hyperpycnal (over density) flows and deposits. Journal of Palaeogeography, 9: 1–21.

Zhang, S.W., Wang, Y.M., and Li, Q., 2003. Searching subtle traps using the theory of slope break. Petroleum Exploration and Development, 30(3): 5–7 (in Chinese with English abstract).

Zhang, W.Z., Zha, M., Hang, H.W., Yu, J.Q., Cui, S.L., and Qu, Z.P., 2017. Quantitative research of coupling relationship between boundary fault activity and sedimentary evolution in Dongying Depression. Journal of China University of Petroleum (Edition of Natural Science), 41(4): 18–26 (in Chinese with English abstract).

Zhang, X., Zhu, X.M., Lu, Z.Y., Lin, C.S., Wang, X., Pan, R., Geng, M.Y., and Xue, Y., 2019. An early Eocene subaqueous fan system in the steep slope of lacustrine rift basins, Dongying Depression, Bohai Bay Basin, China: Depositional character, evolution and geomorphology. Journal of Asian Earth Sciences, 171: 28–45.

Zhong, X.Y., Liu, L.Y., Wang, H.M., Xu, Z.Y., Chen, H., Wang, X.W., and Zhu, Y.S., 2022. Characteristics and origins of the modal pore throat structure in weakly cemented sandy conglomerate reservoirs. Journal of Petroleum Science and Engineering, 208: 109470.

Zhu, J.C., Zou, C.N., Feng, Y.L., Jiang, S., Wu, W.A., Zhu, R.X., and Yuan, M., 2020. Distribution and controls of petroliferous plays in subtle traps within a Paleogene lacustrine sequence stratigraphic framework, Dongying Depression, Bohai Bay Basin, Eastern China. Petroleum Science, 17: 1–22.

Zhu, X.M., Pan, R., Li, S.L., Wang, H.B., Zhang, X., Ge, J.W., and Lu, Z.Y., 2018. Seismic sedimentology of sand-gravel bodies on the steep slope of rift basins—A case study of the Shahejie Formation, Dongying Sag, Eastern China. Interpretation- A Journal of Subsurface Characterization, 6: SD13–SD27.

About the first author

YANG Baoliang, male, born in 1988 in Binzhou, Shandong Province; Ph.D. candidate at China University of Petroleum (East China). He is mainly engaged in sedimentology and sequence stratigraphy. E-mail: yangbl564@163.com.

About the corresponding author

QIU Longwei, born in 1967 in Jiangxi Province, professor and Ph.D. supervisor in School of Geosciences, China University of Petroleum (East China). He is mainly engaged in mineralogy and petrology, sedimentology and reservoir geology. E-mail: qiulwsd@163.com.